Title: Analytical improvements and assessment of long-term performance of the oxidation-denitrifier method

Authors: Simone Moretti[1,2] *#, Nicolas N. Duprey[1]#, Alan D. Foreman[1]#, Anthea Arns[1], Sven Brömme[1], Jonathan Jung[1], Xuyuan E. Ai[1,3], Alexandra Auderset[1,4], Aaron L. Bieler[1], Camino Eck[1], Jesse Farmer[1,3,5], Barbara Hinnenberg[1], Matthew Lacerra[1,3], Jennifer Leichliter[1], Tina Lüdecke[1], Sergey Oleynik[3], Florian Rubach[1], Mareike Schmitt[1], Marissa Vink[1], Tanja Wald[1], Maayan Yehudai[1], Daniel M. Sigman[3], Alfredo Martínez-García[1]*

Affiliations:

[1] Max Planck Institute for Chemistry, Climate Geochemistry Department, Mainz, Germany

[2] Istituto di Scienze Polari, Consiglio Nazionale delle Ricerche, Bologna, Italy

[3] Princeton University, Princeton, New Jersey, United States

[4] University of Southampton, Southampton, United Kingdom

[5] University of Massachusetts Boston, Boston, Massachusetts, United States

* Corresponding authors email: simone.moretti@mpic.de and a.martinez-garcia@mpic.de

# Authors contributed equally

ABSTRACT:

RATIONALE The analysis of the nitrogen (N) isotopic composition of organic matter bound to fossil biomineral structures (BB-$\delta^{15}N$) using the oxidation-denitrifier (O-D) method provides a novel tool to study past changes in N cycling processes.

METHODS We report a set of methodological improvements to the O-D method, including: (i) a method for sealing the reaction vials in which oxidation of organic N to NO_3^- takes place; (ii) a recipe for bypassing the pH adjustment step before the bacterial conversion of NO_3^- to N_2O; and (iii) a storage method of recrystallized dipotassium peroxodisulphate ($K_2S_2O_8$) under Ar atmosphere.

RESULTS The new method eliminates the occasional contamination and vial breakage, and increases sample throughput. The protocol for bypassing of pH adjustment does not affect BB-$\delta^{15}N$, and it significantly reduces processing time. Storage of $K_2S_2O_8$ reagent under Ar atmosphere produces stable oxidation blanks over more than two years. We report analytical blanks, accuracy and precision for this methodology from eight users over the course of ~ 3.5 years of analyses at the Max Planck Institute for Chemistry. Our method produces analytical blanks characterized by low N content (0.30 ± 0.13 nmol N, 1σ, n=204) and stable $\delta^{15}N$ (– 2.45 ± 3.50 ‰, n=204). The analysis of reference amino acid standards USGS40 and USGS65 indicates an overall accuracy of – 0.23 ± 0.35 ‰ (1σ, n=891). The analysis of in-house fossil standards gives similar analytical precision (1σ) across a range of BB-$\delta^{15}N$ values and biominerals: zooxanthellate coral standard PO-1 (6.08 ± 0.21 ‰, n=267), azooxanthellate coral standard LO-1 (10.20 ± 0.28 ‰, n=258), foraminifera standard MF-1 (5.92 ± 0.28 ‰, n=243) and tooth enamel AG-Lox (4.06 ± 0.49 ‰, n=78).

CONCLUSIONS The proposed analytical improvements significantly increase sample throughput without compromising analytical precision or accuracy down to 1 nmol of N.

Keywords: Nitrogen isotopes, denitrifier method, fossil-bound $\delta^{15}N$, biominerals, biomineral organic matter

INTRODUCTION

The natural variation in the ratio of the Nitrogen isotopes (i.e., the $^{15}N/^{14}N$ ratio) has been used extensively over the last decades to trace a vast array of biologically-mediated transformations of this element in modern terrestrial and marine environments (Deniro and Epstein, 1981; Ambrose, 1986; Casciotti, 2016; Sigman and Fripiat, 2019; Ferrier-Pagès and Leal, 2019). Despite an early recognition of the potential utility of N isotopes for elucidating past changes in both the N cycle and past food webs, their application to the fossil record was initially hindered by the low concentrations of organic N typically found in biominerals (typically 1–10 nano(n)mol/mg). This range of concentrations imposed an analytical barrier for the analysis of biominerals using conventional measurement techniques (e.g. Elemental Analyzer coupled to Isotope Ratio Mass Spectrometry), which normally have required sample sizes in the micro(μ)-mole range (Qi et al., 2003; Schimmelmann et al., 2016).

The advent of the denitrifier method in 2001 first allowed for analysis of the nitrogen and oxygen isotopic composition (hereafter $\delta^{15}N$ and $\delta^{18}O$, where $\delta^{15}N = [((^{15}N/^{14}N)_{sample} / (^{15}N/^{14}N)_{atmN2}) - 1) \times 1000]$ and $\delta^{18}O = [((^{18}O/^{16}O)_{sample} / (^{18}O/^{16}O)_{VSMOW}) - 1) \times 1000]$) of seawater and freshwater NO_3^- at nmol concentrations (Sigman et al., 2001; Casciotti et al., 2002). Briefly, the denitrifier method relies on the use of denitrifying bacteria that lack nitrous oxide reductase activity, *Pseudomonas chlororaphis* (ATCC# 43928, Manassas, VA, USA) and *Pseudomonas chlororaphis subsp. aureofaciens* (ATCC# 13985, Manassas, VA, USA) (Christensen and Tiedje, 1988), to quantitatively convert NO_3^- to N_2O. Bacterially-produced N_2O is purified and concentrated with a custom-built system and delivered to an IRMS. This method allows for precise and accurate determination of the $\delta^{15}N$ of NO_3^- down to 1–2 nmol of N. For an in-depth discussion on the bacterial preparation, the conversion of NO_3^- to N_2O and its subsequent measurement, the reader is redirected to (Sigman et al., 2001; Casciotti et al., 2002; McIlvin and Casciotti, 2011; Weigand et al., 2016).

The precision and accuracy of the denitrifier method at nmol concentrations prompted a recognition that, by pairing it with an oxidation method that converts organic matter and other reduced N forms to nitrate (Knapp and Sigman, 2003; Knapp et al., 2005), the N isotope composition of organic matter preserved in biominerals could be constrained. Specifically, these authors demonstrated that, by coupling the products of a dipotassium peroxodisulphate ($K_2S_2O_8$) oxidation reaction, first developed by Nydahl (1978) to convert dissolved organic N (DON) species to NO_3^-, with the denitrifier method described by Sigman et al. (2001), they could achieve accurate and precise analysis of the $\delta^{15}N$ of reduced forms of N at nanomole concentrations (Knapp et al., 2005).

This coupled oxidation-denitrifier (O-D) method thus provided a platform by which the precise analysis of the nitrogen isotopic composition of organic N bound in various fossil and modern biogenic minerals could be achieved. With the increasing recognition that the $\delta^{15}N$ of the organic matter enclosed within biominerals is diagenetically robust and reflects the isotopic composition of the host organism's N, the biomineral-bound or BB-$\delta^{15}N$ proxy began to be applied widely for a variety of archives over the last two decades, including foraminifera (Ren et al., 2009, 2012, 2015, 2017; Costa et al., 2016; Straub et al., 2013a; Straub et al., 2013b; Martínez-García et al., 2014; Farmer et al., 2016, 2021, 2023; Kast et al., 2019; Auderset et al., 2022; Wang et al., 2022), deep- and shallow-water scleractinian corals (Muscatine et al., 2005; Wang et al., 2014, 2015, 2016, 2017; Erler et al., 2015, 2018, 2019, 2020; Duprey et al., 2017, 2020; Zinke et al., 2023; DeLong et al., 2023), tooth enamel/enameloid (Leichliter et al., 2021, 2023; Lüdecke et al.,

2022; Kast et al., 2022), and diatoms (Robinson et al., 2004, 2005; Brunelle et al., 2007; Studer et al., 2012, 2013, 2015, 2018; Ai et al., 2020).

The substantial increase in the applications of the O-D method has highlighted the need for procedural improvements to increase sample throughput without losing precision or accuracy. Here we present modifications to the method initially established by Knapp et al (2005) for dissolved organic matter, and further developed by Ren et al (2009) for application to carbonate archives. The improvements we present are aimed at overcoming three difficulties that had previously hampered the application of this method. First, in the original method, each dissolved sample was combined with basic $K_2S_2O_8$ oxidative reagent in a pre-combusted borosilicate glass vial closed with a Teflon lined cap; these vials were prone to leakage, contamination, and/or breakage. Second, following the oxidation step, the high pH of the sample solution (>14) required the samples be acidified prior to their injection to the denitrifying bacteria to minimize disruption to bacterial physiology. This process is sample-specific and time consuming. Last, best practices for storing $K_2S_2O_8$ to minimize its contribution to the oxidation blank have remained an open question, with approaches varying among users and laboratories.

The analytical improvements to the O-D method we present here address these problems, and have allowed us to increase our sample throughput without compromising analytical precision (Fig. 1). We evaluate the long-term inter-user reproducibility of this updated methodology and its performance over a range of 1–20 nmol of N over three years of observations at the Max Planck Institute for Chemistry (MPIC).

2 EXPERIMENTAL

2.1 Analytical improvements to the oxidation-denitrifier method

The general methodology used in this study is based on the O-D methods developed for the analysis of foraminifera (Ren et al., 2009), stony corals (Wang et al., 2014) and tooth enamel (Leichliter et al., 2021) samples. In order to optimize the sample throughput, three modifications were introduced:

(i) *Vial rack for the oxidation step ("sandwich").* The standard phenolic caps used to seal the 4 ml borosilicate glass vials for the oxidation step by Knapp et al. (2005) were the only off-shelf product able to maintain adequate sealing over an autoclave cycle (120 ℃), and have been a crucial consumable used in this method over the last two decades. These caps come with a major drawback, however, as the phenolic material tends to degrade quickly when exposed to heat and water, becoming brittle and leaching out N containing compounds. To prevent contamination, a thin rubber liner coated with Polytetrafluoroethylene (PTFE) is fit inside each cap. Clearly-contaminated samples occur sporadically when these caps are used, which can be identified by their anomalously-high N content, although the possibility of lower level contamination across a greater number of samples is more difficult to assess. The addition of an extra oxidatively-cleaned PTFE liner between the cap and the sample vial significantly decreased the number of contaminated samples, but did not completely eliminate their occurrence.

In addition, single-use phenolic caps required substantial pretreatment prior to sample oxidation. Each cap first had to be pre-rinsed with milliQ water and dried, and the single use pre-

cut PTFE liners had to be oxidized with a solution of $K_2S_2O_8$ and NaOH, rinsed with milliQ water, and dried. Finally, the two had to be manually assembled by each user before oxidation.

To reduce occasional contamination from the phenolic caps and increase sample throughput, we designed a rack in which the vials are placed open in an aluminum holder and closed by a single 0.1mm PTFE sheet and a 2 mm silicone mat (Fig. 2). The rack is then "sandwiched" between two 14 mm-thick aluminum plates and held in place with bolts and nuts to seal the PTFE and silicone layers atop the oxidation vials, thereby preventing leaks and atmospheric contamination (Supplementary Fig. S1). This design allows the oxidation step to proceed without the need of phenolic caps. After the autoclaving, vials can be capped with regular polypropylene caps, as organic contaminants are no longer an issue once the oxidation reaction to NO_3^- has taken place and the reagent is exhausted. This new method for sealing the reaction vials eliminates the occasional contamination of samples from vial caps and increases the number of samples that can be oxidized in one sample batch (80 samples as per current methodology), without compromising analytical precision or accuracy (See Section 3). We provide a full 3D Model of the assembly in STEP format in the Supplementary Data.

(ii) *Bypassing the pH balancing step.* The need for the oxidizing solution to remain basic during the autoclave step (Nydahl, 1978) means that each oxidized sample has an elevated pH (13–14) that could potentially alter bacterial physiology if injected without acidification. Previously, this step was carried out by iterations of incremental addition of small (1-5µl) amounts of 4 molar hydrochloric acid (4M HCl) to the solution. After each addition, the pH of the sample was tested by manually transferring a small amount (~ 15µl) of sample solution to a pH strip. In case of excessive addition of HCl, the pH had to be elevated back to physiological values via addition of 2M NaOH. This step is time-consuming (e.g., 5–8 hours for 80 samples) and can lead to up to 10% of sample solution being consumed during pH testing. Previously, both the 4M HCl solution used to dissolve the biomineral sample and the NaOH solution were made on the same day of the oxidative step from an ultrahigh purity (Fisher Optima™ grade) 12M HCl mother stock and NaOH pellets, respectively, in order to minimize contamination. This added further time requirements for the pH balancing step. Below, we describe updates to the method aimed at bypassing the pH balancing by (1) standardizing the amount of NaOH added during the oxidation step, and (2) by optimizing the buffer capacity of the bacterial medium.

The first of these is aimed at standardizing the preparation of the "persulfate oxidizing reagent" (POR) solution used in the oxidation step (Knapp et al., 2005; Ren et al., 2009). We do so in order to constrain and minimize the amount of excess NaOH (the amount of residual NaOH in a sample) in solution after the oxidation, while still ensuring that enough NaOH remains to compensate for the protons generated during the decomposition of the $K_2S_2O_8$ (Nydahl, 1978). We achieved standardization of the POR solution by preparing batches of single-use 10ml aliquots of 4M HCl for mineral dissolution, and batches of single-use 10 ml aliquots of concentrated NaOH solution for preparing the high-pH POR solution. The 4M HCl aliquots were prepared by diluting a mother solution of 12M HCl (Table 1). The aliquots of 4M HCl were stored in 12ml pre-combusted borosilicate glass vials at – 20 ℃. A constant amount of 45 µl of this 4M HCl is added to each sample for demineralization, so a single 10 ml vial is enough to dissolve an entire sample batch of 80 samples (5–8 mg $CaCO_3$) and 20 standards. The NaOH solution for the POR was prepared at a concentration of 6.25 µM and split into 10 ml single-use aliquots kept into 15ml polypropylene tubes stored at – 20 ℃. A fixed volume of 4 ml of this 6.25 µM NaOH solution was taken from the single-use aliquot and mixed with 96 ml of milliQ water. Finally, 0.7 g of recrystallized $K_2S_2O_8$ were added into that mixture (Table 1). 1 ml of POR was amended into each

sample, vials were sealed using the new vial rack, and placed in the autoclave at 120 ℃ for 65 minutes. The use of pre-made single-use aliquots of HCl and NaOH for sample acidification and preparation of the POR significantly reduces intra-user variability and reduces processing times.

The second improvement we describe here involves altering the buffering capacity of the *P. chlororaphis* resuspension media used in the denitrifier method so that more than 60 ± 4 µmol of NaOH can be added without increasing the pH beyond the upper range of the bacterial optimum, i.e., pH 7.5 (Bodelier et al., 1997). For this purpose, we used a resuspension media recipe buffered at pH 6.3 made with potassium phosphate monobasic (KH_2PO_4), instead of potassium phosphate dibasic (K_2HPO_4) (Casciotti et al., 2002; Weigand et al., 2016). In addition to changing the recipe, we tested whether using more resuspension media per headspace vial (3 ml) than previous studies (1 to 1.5 ml; Ren et al., 2009, Wang et al., 2014, Weigand et al., 2016) had an impact on the precision and accuracy of the results; a larger volume of buffered resuspension media provides an increased buffering capacity per headspace vial for each bacterial sample.

To constrain the altered buffering capacity of the new resuspension media recipe and the impact of the increased volume of resuspension media per headspace vial, we measured the pH of freshly harvested *P. chlororaphis* bacteria resuspended in the pH 6.3 media injected with between 0 and 1000 µl of non-pH adjusted oxidized solutions with varying excess NaOH concentration (Section 3.1). The oxidized solutions contained 0 (oxidation blanks and amino acid standards), 2, 4 and 8 mg of the in-house coral standard PO-1 (Table 2). The oxidation, the bacterial harvest, the bacteria resuspension and the injection to the headspace vials were carried out following the same protocol used for coral samples (Wang et al., 2015; Weigand et al., 2016).

(iii) *Recrystallized $K_2S_2O_8$ storage*. The highly oxidative properties of $K_2S_2O_8$ mean that it is likely to convert any form of reactive N present in the laboratory environment to NO_3^-. As such, it has the potential to contribute substantially to oxidation blanks in the O-D method given its essential role in the oxidation step and its tendency to bear significant N (Nydahl, 1978). To address this issue, off-shelf reagent-grade $K_2S_2O_8$ is typically recrystallized four times prior to use in order to reduce oxidation blanks (Knapp et al., 2005). This process is time-consuming, and, although the recrystallized $K_2S_2O_8$ is typically stored in a desiccator, past users have reported that oxidation blanks tend to increase within weeks after recrystallization. Therefore, freshly recrystallized $K_2S_2O_8$ is typically used only for a maximum of 3 months after recrystallization.

To improve the useful lifetime of the recrystallized $K_2S_2O_8$ reagent, we tested the storage of freshly re-crystallized $K_2S_2O_8$ in 0.8-1 g aliquots under argon (Ar) atmosphere in 20 ml EPA glass vials vacuum-sealed inside an aluminum coated bag (Supplementary Fig. S2). Each aliquot is used only once to minimize the exposure of the clean reagent to lab air and moisture. We provide a full 3D model in STEP format of the apparatus used to replace the atmosphere in the EPA vials with Ar in the Supplementary Data.

The three changes described above represent a substantial improvement in sample throughput for the O-D method, but whether any of them alter the precision or accuracy of the O-D method remains an open question. To evaluate the potential impact of the changes in the O-D method described above, eight individual users reported $\delta^{15}N$ and N content measurements of oxidation blanks, international reference materials (RMs, also called standards) amino acids and in-house biomineral RMs over the course of ~ 3.5 years.

2.2 Data correction and estimation of accuracy and precision

Conversion of $\delta^{15}N$ IRMS data from the denitrifier method to an international RM (*vs.* air) is a two-step process. First, N_2O measurements are normalized against an N_2O tank that is analyzed in parallel to sample N_2O for each sample. Second, they are normalized to air on a true-vs-analyzed $\delta^{15}N$ scale using two potassium nitrate (KNO_3) standards: USGS 34 [The National Institute of Standards and Technology, Gaithersburg, MD, USA (– 1.8 ± 0.2 ‰)] and IAEA-NO3 [International Atomic Energy Agency, Vienna, Austria (+ 4.7 ± 0.2 ‰)] (Sigman et al., 2009). Although this normalization accounts for offsets introduced during measurement and the denitrifier step of the method, it does not take into account blanks introduced during the oxidation step.

To solve this problem, the N content and $\delta^{15}N$ of the blank from the oxidation step onwards are measured directly and subtracted from each individual measurement using a simple two end-member mixing model. While the measurement of the isotopic composition of the blank in a single vial is not possible due to the extremely low N content of oxidation blanks (~ 0.3 nmol, see Section 3.2), it can be achieved by combining 4–5 individual 1 ml oxidation blanks to achieve a combined blank size of 1 to 2 nmol of N. N contents in this range (1-3 nmol) require additional empirical correction due to a combination of machine noise and an increase in the relative fraction of bacterial N introduced to the sample (Weigand et al., 2016). The combined blank measurement was thus corrected by quantifying the offset from the true value of USGS 34 and IAEA-NO3 in the size range of oxidation blanks (from 0.5 to 3 nmol, Supplementary Fig. S3) and removing this offset from the blank $\delta^{15}N$ measurements. The N content and $\delta^{15}N$ of the blank was then incorporated in a two end-member mixing model correction that takes into account the size and $\delta^{15}N$ of the oxidation blank, and was applied to all oxidized samples and RMs ($\delta^{15}N_{measured} = \delta^{15}N_{sample}\ (1- f_{blank}) + \delta^{15}N_{blank} \cdot f_{blank}$).

To estimate the accuracy and precision of the modified O-D method we present above (Section 2.1), we used international RMs amino acids USGS 40 and 65 (Table 2) normally measured in each sample batch. It is essential to note that, unlike other studies (Ren et al., 2009; Straub et al., 2013; Martínez-García et al., 2014; Wang et al., 2016), in this work these amino acid RMs were not used for blank $\delta^{15}N$ estimation and, therefore, can be used to independently monitor the accuracy and precision of the method from the oxidation step onwards.

To date, a method to directly measure the full procedural blank, that is, accounting for both the oxidation blank and also the potential contribution of the biomineral cleaning step, is lacking. This is due to the fact that the quantification of such a contribution would require a representative biomineral with no N content. Such material is not easily obtainable; even abiotic carbonates reveal small but significant amount of residual N during in-house testing. In-house experiments at MPIC attempted to artificially create such material by heating different biomineral powders at 100-500 ℃; however, these experiments were unable to completely remove all organic N without destroying the biomineral matrix (Martínez-García et al., 2022). Thus, the long-term precision of the complete O-D method, as well as the potential contribution of any procedural blank introduced during the cleaning step, was quantified using in-house biomineral RMs that were cleaned and analyzed in each sample batch (Table 2).

3 RESULTS AND DISCUSSION

In this section we describe $\delta^{15}N$ and N content results of analyses of international and in-house RMs from 8 users over the span of 3.5 years, and evaluate the precision and accuracy of the O-D method using the changes described above. We begin by describing the buffering characteristics of the altered resuspension media, and demonstrate that the addition of non-acidified samples to this new media provides results which are statistically indistinguishable from acidified (i.e. 'pH-balanced') samples (Section 3.1). Next, we show that the oxidation blanks produced by the adapted O-D method are both stable and consistently low across the entire measurement period (Section 3.2) across 8 users. We demonstrate that the changes in the storage method of $K_2S_2O_8$ produce blanks which are consistent and stable over the entire 2.5 year period which we tested (Section 3.2). Last, we evaluate the long term accuracy and precision of international RMs (Section 3.3) and in-house biomineral RMs (Section 3.4), and demonstrate that we can achieve methodological precision down to 1 nmol of N (Section 3.5).

3.1 Bypassing pH adjustment

The oxidations described in this and any following sections were performed using the apparatus detailed in section 2.1 (i) and Fig. 1. As described in Section 2.1 (ii), we evaluated the buffering capacity of the bacteria resuspension media to determine the range in sample size that could be added to a bacterial vial without the need for pH adjustment. 1000 µl of solution of samples with 0 (oxidation blank), 2, 4 and 8 mg of dissolved and oxidized coral samples had an equivalent of 11, 14, 28 and 56 µmol of excess NaOH respectively. Adding each of these to 3 ml of bacteria resuspension media buffered at pH 6.3, resulted in the following pH changes: 6.58, 6.69, 6.83 and 6.97. This range of pH is well within the optimal pH range reported for *P. chlororaphis* (pH 6.3–7.5; Fig. 3A), meaning that optimal conditions for full conversion of the sample NO_3^- into N_2O can be achieved across a wide range of sample sizes. It is worth noting that, in previous studies, the bacteria cultures were resuspended in a media buffered at pH 7.3 for *P. chlororaphis* (Weigand et al., 2017), a value higher than the highest value reported in this experiment (pH 6.97).

We repeated the experiment using 1.5 ml of resuspension media instead of 3 ml, to simulate more extreme scenarios with regard to sample size. The highest amount of NaOH (i.e., 56 µmol of excess NaOH, associated with 8 mg of coral powder) amended to 1.5ml of resuspension media resulted in a pH of 7.44 (Fig. 3B), which it is still lower than the upper pH range for *P. chlororaphis* pH optimum, highlighting the large buffering capacity of the media used. We therefore chose to routinely use 2.75 to 3 ml of resuspension media for each sample for experiments spanning the last 3.5 years to ensure a higher buffering capacity. The higher bacterial media-to-sample volume ratio has the additional benefit of minimizing the local loss of bacteria upon sample injection prior to homogenization of the vial by shaking.

We next evaluated whether bypassing the pH adjustment led to significant differences in sample $\delta^{15}N$ and weight-normalized N content values relative to the previous protocol that included pH adjustment (Knapp et al., 2005). For this test we processed two in house calcium carbonate ($CaCO_3$) coral RMs (PO-1, LO-1), one international amino acid RM (USGS 40) and as well as a set of scleractinian coral samples (*Pocillopora damicornis*). For all materials, each sample was analyzed twice in the same batch, one with pH adjustment, and one without.

A cross-plot of the results obtained with the two methodologies yields a regression line which is statistically undistinguishable (95% confidence envelope) from a theoretical 1:1 line (Fig.

4A), suggesting no difference for both $\delta^{15}N$ and weight-normalized N content in all sample and RM types. The median of the differences between the paired samples for each treatment was always < 0.2 ‰ for $\delta^{15}N$ and < 0.1 nmol/mg for weight-normalized N content (Fig. 4B, Table 3). A two-tailed unpaired t-test (α<0.05) between whole dataset means of paired pH adjusted and non pH adjusted amino acids, PO-1 and LO-1 RMs and coral samples (Table 3), further shows no statistically-significant difference between methods (P>0.05 in all cases). These results demonstrate that bypassing the pH adjustment does result in a statistically significant offset in either $\delta^{15}N$ and weight-normalized N content with respect to samples processed with former method. We therefore conclude that oxidized NO_3^- samples can be injected directly to denitrifying bacteria using 2.75 to 3 ml of resuspended bacteria media buffered with KH_2PO_4. Although this requires a larger amount of bacteria solution per sample, bypassing the pH adjustment step simplifies the procedure and significantly reduces user laboratory time (by as much as 5-8 hours, depending on the batch size). All RM data (amino acid and biomineral) presented in the following sections were obtained by injection to bacteria bypassing the pH balancing step, as described above. While it is likely that oxidation blanks could also be injected directly to the bacteria, we chose to acidify these samples because they require the combination of 5 individual aliquots of oxidizing solution, and would thus be closer to the upper limit of the envelope of optimal pH conditions of *P. Chlororaphis* (Fig. 3). Thus, all blanks data presented in the next sections of this study work were processed following this approach.

3.2 Long term stability of oxidation-denitrifier oxidation blanks

The updated method (Fig. 1) produced consistent oxidation blanks (hereafter referred to as blanks) among users over 4 years, characterized by low N content and relatively stable $\delta^{15}N$ values. The laboratory mean of all blanks measured by eight users following the modified protocol in the period from 2019 to 2023 yielded a $\delta^{15}N$ of – 2.45 ± 3.50 ‰ (n=204) and a blank N content of 0.30 ± 0.13 nmol (n=204) (Fig. 5, Table 4). A one-way Anova test found no statistically significant user differences for $\delta^{15}N$ when compared to the whole-laboratory mean except for user 5. N content differences among users with were generally not statistically significant, with the exception of user 3 (Fig. 5, Supplementary Fig. S4).

We did not observe clear long-term trends in the size or $\delta^{15}N$ of the blanks. Instead, our blanks showed day-to-day variability, even for the same user. We hypothesized that the variability of blank $\delta^{15}N$ and N content could be related to variable contributions from ^{15}N-depleted atmospheric NH_3 on different days. This is supported by data presented in Supplementary Fig. S5, which shows results from in-house exposure tests (0 – 120 minutes) of oxidation vials to air inside a clean room where all oxidations are performed, which is equipped with an activated carbon and particle filter (GCS GmbH, 742x742x96 mm) to minimize exposure to airborne N species. We tested vials containing 4M HCl, which should maximize the trapping of atmospheric NH_3, and HCl + POR, which should be more representative of the blank of a typical sample. In general, longer aerial exposure of both HCl and HCl + POR resulted in a progressive increase in N content and a decrease in blank $\delta^{15}N$ (Supplementary Fig. S5), but the N content and $\delta^{15}N$ for a given exposure time was different on different days. These results are consistent with an increased contribution of atmospheric NH_3 to the blanks with increased exposure time. However, in a typical sample batch the average user-reported exposure time during the oxidation step rarely exceeded 15 minutes, so the impact of atmospheric NH_3 should have been relatively low (Supplementary Fig. S6). In addition, we did not observe a clear correlation between N content and $\delta^{15}N$ in the

blanks analyzed over the past 3.5 years (Supplementary Fig. S6). This suggest that the variability in the $\delta^{15}N$ of the blank may be related to changes in the relative contribution of different blank sources on different days.

In most cases the contribution of the blank to the measured $\delta^{15}N$ is minimal. For example, in a typical biomineral sample containing 10 nmol of N, the average blank of the lab (0.3 nmol and – 2.45 ‰) would represent a fractional contribution of the blank (F_{blank}) of 3 %. If the sample had a non-corrected $\delta^{15}N$ value of 5.0 ‰, the blank-corrected sample $\delta^{15}N$ value would be 5.2 ‰ (Fig. 6). Alternatively, if the N content of the sample was very low, or the amount of available sample material was limited, the fraction of the blank would increase, and consequently the blank correction would be larger for any given blank $\delta^{15}N$ (Fig. 6). A larger correction would also be needed in case that the difference between the $\delta^{15}N$ was larger, e.g. in samples with very high $\delta^{15}N$. In section 3.5, we evaluate the potential effect of a proportionally larger blank on the overall precision of the method by measuring our coral and foraminifera in-house RMs at low N concentrations.

3.2.1 Dipotassium peroxodisulphate storage and its effect on oxidation blanks

The conventional storage method for recrystallized $K_2S_2O_8$ in a desiccator reportedly resulted in a progressive increase in the N content of blanks after over just few months of storage. It has been suggested that highly hygroscopic $K_2S_2O_8$ crystals would adsorb atmospheric H_2O during storage, causing partial dissolution and the formation of sulfuric acid onto their surfaces (Nydahl, 1978), therein creating micro-acidic environments. Such microscopic environments would work to trap atmospheric NH_3 (as well as amines and potentially other N compounds) by diffusion, eventually affecting the blank. We therefore stored individual aliquots of $K_2S_2O_8$ under Ar to prevent the adsorption of H_2O. As a further precaution, we stored these aliquots in Aluminum-lined vacuum bags. Long-term testing of $K_2S_2O_8$ crystals stored in this manner for ~ 2.5 years (Section 2.3) showed that POR blank N content remained very low (≤ 0.3 nmol) over this timespan (Fig. 7B). At the end of the Ar storage experiments, the N content of the blank was indistinguishable from the initial values or the whole-laboratory mean (Fig. 7B), where users typically report the use of $K_2S_2O_8$ (stored under Ar atmosphere) up to a maximum of three months. Blank $\delta^{15}N$ values after ~ 2.5 years of storage are likewise indistinguishable from the mean laboratory values (Fig. 7A). The two initial $\delta^{15}N$ values at the beginning of the experiment are significantly higher than the mean of all the blanks analyzed by all users in the period 2019–2023 ($p<0.05$ for a double tailed unpaired t-test) (Fig. 7A). However, comparing the dates in which those blanks were analyzed to the whole-laboratory timeseries reveals that the sample distribution lies well within the range of observed blank $\delta^{15}N$ values and the lack of increase of N content with time further suggests that the apparent trend cannot be associated with an accumulation of contaminant on the recrystallized $K_2S_2O_8$ reagent.

3.3 Long-term accuracy of international isotopic reference materials

Analysis of international reference amino acid RMs allows us to reconstruct the methodological accuracy of the O-D method in use at MPIC with respect to $\delta^{15}N$. The inter-user average of all RMs measured in the period from 2019 and 2023 yielded a mean $\delta^{15}N$ of – 4.69 ± 0.32 ‰ (n=491) for USGS 40 and a mean $\delta^{15}N$ of 20.38 ± 0.36 ‰ (n=400) for USGS 65 (Fig. 8;

Table 4). Over the same time period, the average offset from the reported international reference values (Qi et al., 2003; Schimmelmann et al., 2016) for both RMs combined is – 0.23 ± 0.35 ‰.

A one-way Anova test for USGS 40 revealed no statistically significant differences for all users when compared to the whole-laboratory mean $\delta^{15}N$ (Supplementary Fig. S7). For USGS 65, the same test revealed a barely significant difference for users 3 and 6. The measured offset of both USGS 40 and 65 from their respective reference values is generally indistinguishable across users with a one-way Anova test, with the exception of user 1 and 3 (Supplementary Fig. S7). Overall this suggests a good consistency across users. The slightly higher standard deviation of USGS 65 (± 0.36 ‰) with respect to USGS 40 (± 0.32 ‰), may be ascribable to its larger $\delta^{15}N$ difference from the blank (20.68‰ *vs.* – 2.45 ‰) (Fig. 6).

The uncertainty reported for both USGS 40 (Qi et al., 2003) and USGS 65 (Schimmelmann et al., 2016) is ± 0.06 ‰. However, in the case of USGS 40 the uncertainty was reported as the average of standard deviations across five measurement sessions from 2 laboratories. For USGS 65, the uncertainty is based on Bayesian Random Effect statistical analysis on data contributed by 9 different laboratories. For comparability with our $\delta^{15}N$ measurements, we recalculated the standard deviation of the interlaboratory mean of these RMs with the same error propagation starting from the mean of the individual laboratories results. We obtain a reference material uncertainty of ± 0.15 ‰ for USGS 40 and ± 0.36 ‰ USGS 65, which are displayed in Fig. 9.

It is worth noting that international reference $\delta^{15}N$ values of the amino acid RMs utilized here have been analyzed with conventional elemental-analyzer (EA) techniques (Qi et al., 2003; Schimmelmann et al., 2016), and thus required ~100 µmol of N for measurement. The values reported here for the same RMs using the O-D method are based on sample size in the 1–20 nmol range (Section 3.6) that are three orders of magnitude smaller (Supplementary Fig. S8). Thus, our results indicate that our method produced data with a temporally-consistent accuracy and precision. Since our average values and the reference values are within 1σ analytical precision of each other (Fig. 9), we do not apply any correction for this small offset.

3.4 Long term consistency of biomineral-bound $\delta^{15}N$ and N-content in biomineral in-house reference materials

The analysis of organic N bound in the crystalline structure of biominerals requires that any given sample be chemically pre-cleaned to remove non-bound exogenous organic matter, given the potential for large differences in $\delta^{15}N$ between these two pools of organic N (Sigman et al., 1999; Martínez-García et al., 2022). However, the choice of appropriate chemical cleaning is dependent on both the type of biomineral analyzed, the types of contamination expected, and the diagenetic conditions the biomineral and its sediment matrix have experienced. For example, opaline diatoms dissolve under basic conditions, and thus require that cleaning occur under acidic conditions. Consistent with this expectation, cleaning with perchloric acid of diatom opal gives more reproducible, stable results than cleaning with Na-hypochlorite (NaOCl), which generates a basic solution (Sigman et al., 1999). For foraminifera, which are composed entirely of calcite, Ren et al., (2009) showed that a reductive cleaning followed by either NaOCl or POR oxidative cleaning gave equivalent results for both BB-$\delta^{15}N$ and weight-normalized biomineral N content (nmol of N per milligram of cleaned biomineral material). Since then, POR cleaning has been the predominant choice for foraminifera-bound $\delta^{15}N$ (Ren et al., 2012; Martínez-García et al., 2014; Kast et al., 2019; Auderset et al., 2022). For corals, similar testing showed negligible differences

across NaOCl and POR oxidative cleaning for both BB-$\delta^{15}N$ and weight-normalized N content (Wang et al., 2016), and NaOCl has been established as commonly used method for both deep-sea scleractinian corals (Wang, 2016) and shallow-water scleractinia (Wang et al., 2016; Duprey et al., 2017), with an additional reductive cleaning step for the former, but not the latter. For tooth enamel hydroxyapatite/fluorapatite, a reductive cleaning coupled with a POR oxidative cleaning has commonly been used (Kast et al., 2022; Leichliter et al., 2021). A summary of chemical cleaning methods utilized in this work can be found in Supplementary Table 1.

We have used in-house carbonate and enamel biomineral RMs to evaluate the analytical reproducibility of the O-D method (cleaning, oxidation, injection to bacteria, and measurement by IRMS). The impact of chemical cleaning on the long-term reproducibility is thus implicitly constrained by this measurement; below we detail the results of the analysis of two coral aragonitic materials (PO-1 and LO-1), one calcitic foraminifera RM (MF-1) and one hydroxyapatite RM (AG-Lox) over a ~ 3.5 years period by eight individual users are shown in Fig. 10 and summarized in Table 4.

The analysis of the two coral RMs in the period from 2019 and 2023 yielded a mean inter-user BB-$\delta^{15}N$ of 6.08 ± 0.21 ‰ (n=267) and 10.20 ± 0.28 ‰ (n=258) for NaOCl cleaned PO-1 and LO-1 respectively (Fig. 10, Table 5). The uncertainties reported here for our modified method are compatible with reported values for the previous method at Princeton University (~0.2 ‰) for another in-house coral RM (CBS-1), also cleaned with NaOCl (Wang et al., 2022). PO-1 and LO-1 RMs were also repeatedly cleaned with POR during the same period to compare the two cleaning methods. The inter-user average of PO-1 and LO-1 coral RMs cleaned in this manner yielded a mean BB-$\delta^{15}N$ of 6.14 ± 0.23 ‰ (n=183) and 10.10 ± 0.29 ‰ (n=272) for POR cleaned PO-1 and LO-1 respectively. Long-term monitoring of CBS-1 coral RM with POR cleaning at Princeton University (Kast et al., 2022) gave a similar reproducibility (± 0.3 ‰) to what we observed with this method. Although the BB-$\delta^{15}N$ differences (POR – NaOCl) are extremely small (0.06 ± 0.31 ‰ for PO-1 and – 0.09 ± 0.40 ‰ for LO-1), the BB-$\delta^{15}N$ of NaOCl-cleaned and POR-cleaned samples are statistically different ($p<0.05$) from each other due to the high number of measurements (Table 5). These differences, which are much smaller than the analytical precision of the O-D method, do not show the same sense of disagreement and can be considered negligible for practical applications.

Significant differences were observed for the weight-normalized N content of these materials across treatments. NaOCl-cleaned PO-1 and LO-1 RMs were consistently lower in weight-normalized N content than those cleaned with POR (Fig. 11, Table 5). The whole-laboratory average of PO-1 in the period from 2019 and 2023 yielded a mean weight-normalized N content of 2.40 ± 0.22 nmol (n=183) for POR cleaning and 1.86 ± 0.20 nmol (n=267) for NaOCl cleaning. The same analysis for LO-1 yielded a mean weight-normalized N content of 2.52 ± 0.24 nmol (n=272) for POR cleaning and 1.44 ± 0.20 nmol (n=258) for NaOCl cleaning (Fig. 10, Table 5). The cause of such an important N content difference remains unclear, particularly when considered alongside an effectively negligible $\delta^{15}N$ difference across treatments for the same coral RMs. One possibility has to do with the mineral structure of PO-1 and LO-1. Scleractinian corals skeleton are mostly composed of aragonite (Von Euw et al., 2017). While stable in ambient conditions, we posit that high-temperatures (120 °C) over the 65 minute autoclave cycle used for POR oxidative cleaning might either induce partial dissolution and recrystallization of the aragonitic mineral matrix of coral RMs (Yoshioka and Kitano, 1985) and/or partial dissolution of the borosilicate vial in the high pH of the POR solution. It remains possible that the formation of secondary mineral or non-crystalline phases during this process might result in trapping of organic

matter, thereby allowing for a greater weight-normalized N content than the same RMs cleaned at room temperature with NaOCl treatment. In Fourier-Transform Infrared Spectroscopy (FTIR) analyses of pristine (uncleaned) and POR-cleaned PO-1 and LO-1 coral $CaCO_3$ RMs, a clear change in the IR-spectrum of coral aragonite can been seen after POR cleaning, but no difference from the pristine RM is observed after NaOCl treatment (Supplementary Fig. S8). The added features in POR-cleaned RMs may be identified as calcium silicate hydrate (CSH) phases based on the FTIR signature (John and Stephan, 2021). This suggests that partial dissolution of the borosilicate vials during POR cleaning is at least partially responsible for the higher N contents, which is consistent with experimental precipitation of CSH from aqueous solutions in similar high pH environments rich in Ca and silica (SiO_2) (Greenberg, 1961). In contrast, the fact that the $\delta^{15}N$ offset between NaOCl and POR cleaning methods was lower than 0.1 ‰ argues that the majority of the N trapped (or added) during POR cleaning is native to the coral, and implies that this process likely occurs when most of the exogenous organic matter has already been removed (Table 5).

Unlike the PO-1 and LO-1 RMs, foraminifera RM MF-1 was only cleaned with POR during the experimental period. The laboratory means of BB-$\delta^{15}N$ and weight-normalized N content for this RM at the end of the 3.5 year observation period were 5.92 ± 0.28 ‰ (n=243) and 3.60 ± 0.35 nmol (n=241) respectively. Before the MF-1 RM became available, reproducibility was assessed as the average standard deviation estimated from the means of duplicate measurements. The average standard deviation of replicated foraminifera-bound $\delta^{15}N$ measurements reported in Ren et al., 2009 (± 0.3 ‰), Martinez-Garcia et al., 2014 (± 0.19 ‰), Ren et al 2017 (± 0.22 ‰) and Farmer et al., 2023 (± 0.22 ‰) are similar to the long-term inter-user reproducibility of our foraminifera RM reported here (± 0.28 ‰; Fig. 10C). It is worth noting that contrary to our reported estimations, the previously published uncertainties were based on replicates of the same samples after cleaning, thereby not representative of the full procedural blank. In light of an increasing number of recent foraminifera studies published with BB-$\delta^{15}N$ over the past decade (Martinez-Garcia et al, 2014; Kast et al., 2019; Studer et al., 2021; Auderset et al, 2022), we propose that the MF-1 foraminifera RM is a valid and representative reference material to monitor both intra and inter-laboratory reproducibility for future foraminifera-based $\delta^{15}N$ studies.

The AG-Lox tooth enamel RM was also only cleaned with POR. The laboratory mean for this RM was 4.06 ± 0.49 ‰ (n=78) for $\delta^{15}N$, and 12.49 ± 1.85 nmol (n=78) for weight-normalized N content (Figs. 10D, 11D). Given the novelty of the application (Leichliter et al., 2021), there are no enamel-bound N comparisons available in the literature, but a shark tooth enameloid in-house RM cleaned with POR at Princeton University (Kast et al., 2022) using the previous methodology yielded a comparable but slightly poorer reproducibility for measurements reported by one user (± 0.7 ‰).

Overall, the results of the analysis of biomineral in-house RMs indicate that our modified method ("sandwich", pH-balance bypass, and $K_2S_2O_8$ storage) can be used to increase sample throughput without compromising analytical precision.

3.5 Method performance at low nitrogen concentrations

As noted above, the value of widely used reference material such as USGS 40 and USGS 65 are reported from users employing an EAs coupled IRMS, which typically requires µmol concentrations of N (Qi et al., 2003; Schimmelmann et al., 2016). The O-D method allows for the analysis of 1–2 nmol amounts analyte N, 3 orders of magnitude lower than conventional EA techniques (Sigman et al., 2001; Knapp et al., 2005; Weigand et al., 2016). However, as the sample size decreases, the relative contribution of the procedural blank increases, and the blank correction becomes larger (Fig. 12). Although measurements in the IRMS are typically performed using around 5nmols of N, we typically target around 10-15 nmols of N in each sample in order to minimize the effect of the blank correction (Fig. 6). In this section, we evaluate the performance of the O-D method over the range of 1 to 20 nmols of N.

We divide our dataset in three categories: 1–5 nmol, 5–10 nmol and 10–20 nmol N. For the amino acids RMs USGS 40 and USGS 65 the values obtained were statistically indistinguishable between all the three categories, demonstrating that our blank correction is robust, even in cases where the contribution of the blank is as high as 10 % (Table 6). For BB-$\delta^{15}N$ measurements of our in-house biomineral RMs, the difference between the mean of these categories was always $\leq$ 0.2 ‰ for all RMs, which lies within the reported 1σ analytical precision of our measurements. This suggest that our blank correction provides a good approximation for the analytical blank of the entire procedure. Although the differences between the different categories are within our analytical uncertainty, in some cases, they are statistically significant. Since no significant differences were observed in the case of the amino acid RMs, this observation suggest that the cleaning step may be introducing a small additional blank. In any case its potential impact on the estimated BB-$\delta^{15}N$ would be minimal even in the case of small samples (i.e. from 0.14 ± 0.37 ‰ to 0.23 ± 0.40 ‰). It is also worth noting that our dataset shows no change in the precision of the measurements across the three different sample size categories analyzed (Fig. 12). Thus, it could be possible to use the in-house RMs to correct for the small offsets observed in the mean values.

4 CONCLUDING REMARKS

The analytical changes outlined here provide improvements to the existing methodology for the analysis of BB-$\delta^{15}N$. These include: (i) a consistent way of sealing the oxidation environment for the conversion of organic N to NO_3^-, (ii) bypassing of the pH adjusting of the NO_3^- solutions to be amended to denitrifying bacteria and (iii) improved storage of $K_2S_2O_8$ crystals used for preparation of the POR reagent. Collectively, these changes results in a methodology that increases sample throughput without compromising analytical precision. We also report the development of, and in-house results from, an ongoing framework for monitoring, future methodological work, and intercalibration, in the form of multiple biomineral reference materials.

Acknowledgments:

We are grateful to Taihun Kim for providing the *Porites sp.* coral material used to generate the PO-1 reference material, and to Anne Lorrain and Valentine Meunier for providing *Pocillopora damicornis* coral samples used for pH balancing experiments (samples collected during the research cruise: IGUANE aboard R/V ALIS, DOI: 10.17600/18000897). We are grateful to Thomas Tütken for providing material for the AG-Lox reference material and to Björn Taphorn for the help in the preparation of the MF-1 reference material. We thank Thomas Leutert, Michelle Meffert, Alina Jaeger, Denise Radermacher and Sitara Schmidt for their help in the laboratory in the early stage of this work. We thank Haojia (Abby) Ren, Xingchen (Tony) Wang, Emma R. Kast and Alexandra Weigand for their continued contributions to and communications about methodological improvements.

Funding:

This study was funded by the Max Planck Society (AMG)

The authors also acknowledge funding from the Deutsche Forschungsgemeinschaft (DFG, German Research Foundation), Project number 468591845 (AMG) – SPP 2299/Project number 44183248, the Emmy Noether Fellowship LU 2199/2-1 (TL) and the Paul Crutzen Nobel Prize Postdoctoral Fellowship (ND).

Author contributions:

Conceptualization: SM, ND, AF, FR, AMG

Methodology: SM, ND, AF, AMG

Investigation: SM, ND, AF, AA, SB, JJ, AA, CE, BH, JL, TL, TW, MY, MV

Visualization: SM, AMG

Funding acquisition: AMG

Project administration: AMG

Supervision: AMG

Writing – original draft: SM, AMG

Writing – review & editing: All authors

Competing interests: Authors declare that they have no competing interests

Data and materials availability: Upon publication, dataset and information regarding experimental setup will be uploaded on the journal website and available for download.

Supplementary Materials:

Figs. S1 to S8

Data S1 to S3

REFERENCES:

Ai, X.E., Studer, A.S., Sigman, D.M., Martínez-García, A., Fripiat, F., Thöle, L.M., Michel, E., Gottschalk, J., Arnold, L., Moretti, S., Schmitt, M., Oleynik, S., Jaccard, S.L., Haug, G.H., 2020. Southern Ocean upwelling, Earth's obliquity, and glacial-interglacial atmospheric CO2 change. Science.

Ambrose, S.H., 1986. Stable carbon and nitrogen isotope analysis of human and animal diet in Africa. Journal of Human Evolution 15, 707–731. https://doi.org/10.1016/S0047-2484(86)80006-9

Auderset, A., Moretti, S., Taphorn, B., Ebner, P.-R., Kast, E., Wang, X.T., Schiebel, R., Sigman, D.M., Haug, G.H., Martínez-García, A., 2022. Enhanced ocean oxygenation during Cenozoic warm periods. Nature 609, 77–82. https://doi.org/10.1038/s41586-022-05017-0

Bodelier, P.L.E., Wijlhuizen, A.G., Blom, C.W.P.M., Laanbroek, H.J., 1997. Effects of photoperiod on growth of and denitrification by Pseudomonas chlororaphis in the root zone of Glyceria maxima, studied in a gnotobiotic microcosm. Plant and Soil 190, 91–103. https://doi.org/10.1023/A:1004212814097

Brunelle, B.G., Sigman, D.M., Cook, M.S., Keigwin, L.D., Haug, G.H., Plessen, B., Schettler, G., Jaccard, S.L., 2007. Evidence from diatom-bound nitrogen isotopes for subarctic Pacific stratification during the last ice age and a link to North Pacific denitrification changes. Paleoceanography 22. https://doi.org/10.1029/2005PA001205

Casciotti, K.L., 2016. Nitrogen and Oxygen Isotopic Studies of the Marine Nitrogen Cycle. Annu. Rev. Mar. Sci. 8, 379–407. https://doi.org/10.1146/annurev-marine-010213-135052

Casciotti, K.L., Sigman, D.M., Hastings, M.G., Böhlke, J.K., Hilkert, A., 2002. Measurement of the Oxygen Isotopic Composition of Nitrate in Seawater and Freshwater Using the Denitrifier Method. Anal. Chem. 74, 4905–4912. https://doi.org/10.1021/ac020113w

Christensen, S., Tiedje, J.M., 1988. Sub-parts-per-billion nitrate method: use of an N/sub 2/O-producing denitrifier to convert NO/sub 2//sup -/ or /sup 15/NO/sub 2//sup -/ to N/sub 2/O. Appl. Environ. Microbiol.; (United States) 54:6.

Costa, K.M., McManus, J.F., Anderson, R.F., Ren, H., Sigman, D.M., Winckler, G., Fleisher, M.Q., Marcantonio, F., Ravelo, A.C., 2016. No iron fertilization in the equatorial Pacific Ocean during the last ice age. Nature 529, 519–522. https://doi.org/10.1038/nature16453

DeLong, K.L., Palmer, K., Wagner, A.J., Weerabaddana, M.M., Slowey, N., Herrmann, A.D., Duprey, N., Martínez-García, A., Jung, J., Hajdas, I., Rose, N.L., Roberts, S.L., Roberts, L.R., Cundy, A.B., Gaca, P., Milton, J.A., Yang, H., Turner, S.D., Huang, C.-Y., Shen, C.-C., Zinke, J., 2023. The Flower Garden Banks Siderastrea siderea coral as a candidate Global boundary Stratotype Section and Point for the Anthropocene series. The Anthropocene Review 10, 225–250. https://doi.org/10.1177/20530196221147616

Deniro, M.J., Epstein, S., 1981. Influence of diet on the distribution of nitrogen isotopes in animals. Geochimica et Cosmochimica Acta 45, 341–351. https://doi.org/10.1016/0016-7037(81)90244-1

Duprey, N.N., Wang, T.X., Kim, T., Cybulski, J.D., Vonhof, H.B., Crutzen, P.J., Haug, G.H., Sigman, D.M., Martínez-García, A., Baker, D.M., 2020. Megacity development and the demise of coastal coral communities: Evidence from coral skeleton δ15N records in the Pearl River estuary. Global Change Biology 26, 1338–1353. https://doi.org/10.1111/gcb.14923

Duprey, N.N., Wang, X.T., Thompson, P.D., Pleadwell, J.E., Raymundo, L.J., Kim, K., Sigman, D.M., Baker, D.M., 2017. Life and death of a sewage treatment plant recorded in a coral skeleton δ15N record. Marine Pollution Bulletin 120, 109–116. https://doi.org/10.1016/j.marpolbul.2017.04.023

Erler, D.V., Farid, H.T., Glaze, T.D., Carlson-Perret, N.L., Lough, J.M., 2020. Coral skeletons reveal the history of nitrogen cycling in the coastal Great Barrier Reef. Nat Commun 11, 1500. https://doi.org/10.1038/s41467-020-15278-w

Erler, D.V., Nothdurft, L., McNeil, M., Moras, C.A., 2018. Tracing nitrate sources using the isotopic composition of skeletal-bound organic matter from the calcareous green algae Halimeda. Coral Reefs 37, 1003–1011. https://doi.org/10.1007/s00338-018-01742-z

Erler, D.V., Shepherd, B.O., Linsley, B.K., Nothdurft, L.D., Hua, Q., Lough, J.M., 2019. Has Nitrogen Supply to Coral Reefs in the South Pacific Ocean Changed Over the Past 50 Thousand Years? Paleoceanography and Paleoclimatology 34, 567–579. https://doi.org/10.1029/2019PA003587

Erler, D.V., Wang, X.T., Sigman, D.M., Scheffers, S.R., Shepherd, B.O., 2015. Controls on the nitrogen isotopic composition of shallow water corals across a tropical reef flat transect. Coral Reefs 34, 329–338. https://doi.org/10.1007/s00338-014-1215-5

Farmer, J.R., Hönisch, B., Uchikawa, J., 2016. Single laboratory comparison of MC-ICP-MS and N-TIMS boron isotope analyses in marine carbonates. Chemical Geology 447, 173–182. https://doi.org/10.1016/j.chemgeo.2016.11.008

Farmer, J.R., Pico, T., Underwood, O.M., Cleveland Stout, R., Granger, J., Cronin, T.M., Fripiat, F., Martínez-García, A., Haug, G.H., Sigman, D.M., 2023. The Bering Strait was flooded 10,000 years before the Last Glacial Maximum. Proceedings of the National Academy of Sciences 120, e2206742119. https://doi.org/10.1073/pnas.2206742119

Farmer, J.R., Sigman, D.M., Granger, J., Underwood, O.M., Fripiat, F., Cronin, T.M., Martínez-García, A., Haug, G.H., 2021. Arctic Ocean stratification set by sea level and freshwater inputs since the last ice age. Nat. Geosci. 14, 684–689. https://doi.org/10.1038/s41561-021-00789-y

Ferrier-Pagès, C., Leal, M.C., 2019. Stable isotopes as tracers of trophic interactions in marine mutualistic symbioses. Ecology and Evolution 9, 723–740. https://doi.org/10.1002/ece3.4712

Greenberg, S.A., 1961. REACTION BETWEEN SILICA AND CALCIUM HYDROXIDE SOLUTIONS. I. KINETICS IN THE TEMPERATURE RANGE 30 TO 85°1. J. Phys. Chem. 65, 12–16. https://doi.org/10.1021/j100819a005

John, E., Stephan, D., 2021. Calcium silicate hydrate—in-situ development of the silicate structure followed by infrared spectroscopy. Journal of the American Ceramic Society 104, 6611–6624. https://doi.org/10.1111/jace.18019

Kast, E.R., Griffiths, M.L., Kim, S.L., Rao, Z.C., Shimada, K., Becker, M.A., Maisch, H.M., Eagle, R.A., Clarke, C.A., Neumann, A.N., Karnes, M.E., Lüdecke, T., Leichliter, J.N., Martínez-García, A., Akhtar, A.A., Wang, X.T., Haug, G.H., Sigman, D.M., 2022. Cenozoic megatooth sharks occupied extremely high trophic positions. Science Advances 8, eabl6529. https://doi.org/10.1126/sciadv.abl6529

Kast, E.R., Stolper, D.A., Auderset, A., Higgins, J.A., Ren, H., Wang, X.T., Martínez-García, A., Haug, G.H., Sigman, D.M., 2019. Nitrogen isotope evidence for expanded ocean suboxia in the early Cenozoic. Science 364, 386–389. https://doi.org/10.1126/science.aau5784

Knapp, A.N., Sigman, D.M., 2003. Stable isotopic composition of dissolved organic nitrogen from the surface waters of the Sargasso Sea, in: ASLO Annual Meeting, Salt Lake City, Utah.

Knapp, A.N., Sigman, D.M., Lipschultz, F., 2005. N isotopic composition of dissolved organic nitrogen and nitrate at the Bermuda Atlantic Time-series Study site. Global Biogeochem. Cycles 19, GB1018. https://doi.org/10.1029/2004GB002320

Leichliter, J.N., Lüdecke, T., Foreman, A.D., Bourgon, N., Duprey, N.N., Vonhof, H., Souksavatdy, V., Bacon, A.-M., Sigman, D.M., Tütken, T., Martínez-García, A., 2023. Tooth enamel nitrogen isotope composition records trophic position: a tool for reconstructing food webs. Commun Biol 6, 1–13. https://doi.org/10.1038/s42003-023-04744-y

Leichliter, J.N., Lüdecke, T., Foreman, A.D., Duprey, N.N., Winkler, D.E., Kast, E.R., Vonhof, H., Sigman, D.M., Haug, G.H., Clauss, M., Tütken, T., Martínez-García, A., 2021. Nitrogen isotopes in tooth enamel record diet and trophic level enrichment: Results from a controlled feeding experiment. Chemical Geology 563, 120047. https://doi.org/10.1016/j.chemgeo.2020.120047

Lüdecke, T., Leichliter, J.N., Aldeias, V., Bamford, M.K., Biro, D., Braun, D.R., Capelli, C., Cybulski, J.D., Duprey, N.N., Ferreira da Silva, M.J., Foreman, A.D., Habermann, J.M., Haug, G.H., Martínez, F.I., Mathe, J., Mulch, A., Sigman, D.M., Vonhof, H., Bobe, R., Carvalho, S., Martínez-García, A., 2022. Carbon, nitrogen, and oxygen stable isotopes in modern tooth enamel: A case study from Gorongosa National Park, central Mozambique. Frontiers in Ecology and Evolution 10.

Martínez-García, A., Jung, J., Ai, X.E., Sigman, D.M., Auderset, A., Duprey, N.N., Foreman, A., Fripiat, F., Leichliter, J., Lüdecke, T., Moretti, S., Wald, T., 2022. Laboratory Assessment of the Impact of Chemical Oxidation, Mineral Dissolution, and Heating on the Nitrogen Isotopic Composition of Fossil-Bound Organic Matter. Geochemistry, Geophysics, Geosystems 23, e2022GC010396. https://doi.org/10.1029/2022GC010396

Martínez-García, A., Sigman, D.M., Ren, H., Anderson, R.F., Straub, M., Hodell, D.A., Jaccard, S.L., Eglinton, T.I., Haug, G.H., 2014. Iron Fertilization of the Subantarctic Ocean During the Last Ice Age. Science 343, 1347–1350. https://doi.org/10.1126/science.1246848

McIlvin, M.R., Casciotti, K.L., 2011. Technical updates to the bacterial method for nitrate isotopic analyses. Anal Chem 83, 1850–1856. https://doi.org/10.1021/ac1028984

Muscatine, L., Goiran, C., Land, L., Jaubert, J., Cuif, J.-P., Allemand, D., 2005. Stable isotopes (δ13C and δ15N) of organic matrix from coral skeleton. PNAS 102, 1525–1530. https://doi.org/10.1073/pnas.0408921102

Nydahl, F., 1978. On the peroxodisulphate oxidation of total nitrogen in waters to nitrate. Water Research 12, 1123–1130. https://doi.org/10.1016/0043-1354(78)90060-X

Qi, H., Coplen, T.B., Geilmann, H., Brand, W.A., Böhlke, J.K., 2003. Two new organic reference materials for δ13C and δ15N measurements and a new value for the δ13C of NBS 22 oil. Rapid Communications in Mass Spectrometry 17, 2483–2487. https://doi.org/10.1002/rcm.1219

Ren, H., Sigman, D.M., Martínez-García, A., Anderson, R.F., Chen, M.-T., Ravelo, A.C., Straub, M., Wong, G.T.F., Haug, G.H., 2017. Impact of glacial/interglacial sea level change on the ocean nitrogen cycle. PNAS 114, E6759–E6766. https://doi.org/10.1073/pnas.1701315114

Ren, H., Sigman, D.M., Meckler, A.N., Plessen, B., Robinson, R.S., Rosenthal, Y., Haug, G.H., 2009. Foraminiferal Isotope Evidence of Reduced Nitrogen Fixation in the Ice Age Atlantic Ocean. Science 323, 244–248. https://doi.org/10.1126/science.1165787

Ren, H., Sigman, D.M., Thunell, R.C., Prokopenko, M.G., 2012. Nitrogen isotopic composition of planktonic foraminifera from the modern ocean and recent sediments. Limnol. Oceanogr. 57, 1011–1024. https://doi.org/10.4319/lo.2012.57.4.1011

Ren, H., Studer, A.S., Serno, S., Sigman, D.M., Winckler, G., Anderson, R.F., Oleynik, S., Gersonde, R., Haug, G.H., 2015. Glacial-to-interglacial changes in nitrate supply and consumption in the subarctic North Pacific from microfossil-bound N isotopes at two trophic levels. Paleoceanography 30, 2014PA002765. https://doi.org/10.1002/2014PA002765

Robinson, R.S., Brunelle, B.G., Sigman, D.M., 2004. Revisiting nutrient utilization in the glacial Antarctic: Evidence from a new method for diatom-bound N isotopic analysis. Paleoceanography 19, PA3001. https://doi.org/10.1029/2003PA000996

Robinson, R.S., Sigman, D.M., DiFiore, P.J., Rohde, M.M., Mashiotta, T.A., Lea, D.W., 2005. Diatom-bound 15N/14N: New support for enhanced nutrient consumption in the ice age subantarctic. Paleoceanography 20, PA3003. https://doi.org/10.1029/2004PA001114

Schimmelmann, A., Qi, H., Coplen, T.B., Brand, W.A., Fong, J., Meier-Augenstein, W., Kemp, H.F., Toman, B., Ackermann, A., Assonov, S., Aerts-Bijma, A.T., Brejcha, R., Chikaraishi, Y., Darwish, T., Elsner, M., Gehre, M., Geilmann, H., Gröning, M., Hélie, J.-F., Herrero-Martín, S., Meijer, H.A.J., Sauer, P.E., Sessions, A.L., Werner, R.A., 2016. Organic Reference Materials for Hydrogen, Carbon, and Nitrogen Stable Isotope-Ratio Measurements: Caffeines, n-Alkanes, Fatty Acid Methyl Esters, Glycines, l-Valines, Polyethylenes, and Oils. Anal. Chem. 88, 4294–4302. https://doi.org/10.1021/acs.analchem.5b04392

Sigman, D.M., Altabet, M.A., Francois, R., McCorkle, D.C., Gaillard, J.-F., 1999. The isotopic composition of diatom-bound nitrogen in Southern Ocean sediments. Paleoceanography 14, 118–134. https://doi.org/10.1029/1998PA900018

Sigman, D.M., Casciotti, K.L., Andreani, M., Barford, C., Galanter, M., Böhlke, J.K., 2001. A Bacterial Method for the Nitrogen Isotopic Analysis of Nitrate in Seawater and Freshwater. Anal. Chem. 73, 4145–4153. https://doi.org/10.1021/ac010088e

Sigman, D.M., DiFiore, P.J., Hain, M.P., Deutsch, C., Wang, Y., Karl, D.M., Knapp, A.N., Lehmann, M.F., Pantoja, S., 2009. The dual isotopes of deep nitrate as a constraint on the cycle and budget of oceanic fixed nitrogen. Deep Sea Research Part I: Oceanographic Research Papers 56, 1419–1439. https://doi.org/10.1016/j.dsr.2009.04.007

Sigman, D.M., Fripiat, F., 2019. Nitrogen Isotopes in the Ocean, in: Cochran, J.K., Bokuniewicz, H.J., Yager, P.L. (Eds.), Encyclopedia of Ocean Sciences (Third Edition). Academic Press, Oxford, pp. 263–278. https://doi.org/10.1016/B978-0-12-409548-9.11605-7

Straub, Marietta, Sigman, D.M., Ren, H., Martínez-García, A., Meckler, A.N., Hain, M.P., Haug, G.H., 2013. Changes in North Atlantic nitrogen fixation controlled by ocean circulation. Nature 501, 200–203. https://doi.org/10.1038/nature12397

Straub, M., Tremblay, M.M., Sigman, D.M., Studer, A.S., Ren, H., Toggweiler, J.R., Haug, G.H., 2013. Nutrient conditions in the subpolar North Atlantic during the last glacial period reconstructed from foraminifera-bound nitrogen isotopes. Paleoceanography 28, 79–90. https://doi.org/10.1002/palo.20013

Studer, A.S., Ellis, K.K., Oleynik, S., Sigman, D.M., Haug, G.H., 2013. Size-specific opal-bound nitrogen isotope measurements in North Pacific sediments. Geochimica et Cosmochimica Acta 120, 179–194. https://doi.org/10.1016/j.gca.2013.06.041

Studer, A.S., Martínez-Garcia, A., Jaccard, S.L., Girault, F.E., Sigman, D.M., Haug, G.H., 2012. Enhanced stratification and seasonality in the Subarctic Pacific upon Northern Hemisphere Glaciation–New evidence from diatom-bound nitrogen isotopes, alkenones and archaeal tetraethers. Earth and Planetary Science Letters 351–352, 84–94. https://doi.org/10.1016/j.epsl.2012.07.029

Studer, A.S., Sigman, D.M., Martínez-García, A., Benz, V., Winckler, G., Kuhn, G., Esper, O., Lamy, F., Jaccard, S.L., Wacker, L., Oleynik, S., Gersonde, R., Haug, G.H., 2015. Antarctic Zone nutrient conditions during the last two glacial cycles. Paleoceanography 30, 2014PA002745. https://doi.org/10.1002/2014PA002745

Studer, A.S., Sigman, D.M., Martínez-García, A., Thöle, L.M., Michel, E., Jaccard, S.L., Lippold, J.A., Mazaud, A., Wang, X.T., Robinson, L.F., Adkins, J.F., Haug, G.H., 2018. Increased nutrient supply to the Southern Ocean during the Holocene and its implications for the pre-industrial atmospheric CO2 rise. Nature Geosci 11, 756–760. https://doi.org/10.1038/s41561-018-0191-8

Von Euw, S., Zhang, Q., Manichev, V., Murali, N., Gross, J., Feldman, L.C., Gustafsson, T., Flach, C., Mendelsohn, R., Falkowski, P.G., 2017. Biological control of aragonite formation in stony corals. Science 356, 933–938. https://doi.org/10.1126/science.aam6371

Wang, X.T., 2016. Nitrogen isotopes in scleractinian corals: Modern ocean studies and paleoceanographic applications.

Wang, X.T., Prokopenko, M.G., Sigman, D.M., Adkins, J.F., Robinson, L.F., Ren, H., Oleynik, S., Williams, B., Haug, G.H., 2014. Isotopic composition of carbonate-bound organic nitrogen in deep-sea scleractinian corals: A new window into past biogeochemical change. Earth and Planetary Science Letters 400, 243–250. https://doi.org/10.1016/j.epsl.2014.05.048

Wang, X.T., Sigman, D.M., Cohen, A.L., Sinclair, D.J., Sherrell, R.M., Cobb, K.M., Erler, D.V., Stolarski, J., Kitahara, M.V., Ren, H., 2016. Influence of open ocean nitrogen supply on the skeletal δ15N of modern shallow-water scleractinian corals. Earth and Planetary Science Letters 441, 125–132. https://doi.org/10.1016/j.epsl.2016.02.032

Wang, X.T., Sigman, D.M., Cohen, A.L., Sinclair, D.J., Sherrell, R.M., Weigand, M.A., Erler, D.V., Ren, H., 2015. Isotopic composition of skeleton-bound organic nitrogen in reef-building symbiotic corals: A new method and proxy evaluation at Bermuda. Geochimica et Cosmochimica Acta 148, 179–190. https://doi.org/10.1016/j.gca.2014.09.017

Wang, X.T., Sigman, D.M., Prokopenko, M.G., Adkins, J.F., Robinson, L.F., Hines, S.K., Chai, J., Studer, A.S., Martínez-García, A., Chen, T., Haug, G.H., 2017. Deep-sea coral evidence for lower Southern Ocean surface nitrate concentrations during the last ice age. PNAS 114, 3352–3357. https://doi.org/10.1073/pnas.1615718114

Wang, X.T., Wang, Y., Auderset, A., Sigman, D.M., Ren, H., Martínez-García, A., Haug, G.H., Su, Z., Zhang, Y.G., Rasmussen, B., Sessions, A.L., Fischer, W.W., 2022. Oceanic nutrient rise and the late Miocene inception of Pacific oxygen-deficient zones. Proceedings of the National Academy of Sciences 119, e2204986119. https://doi.org/10.1073/pnas.2204986119

Weigand, M.A., Foriel, J., Barnett, B., Oleynik, S., Sigman, D.M., 2016. Updates to instrumentation and protocols for isotopic analysis of nitrate by the denitrifier method. Rapid Communications in Mass Spectrometry 30, 1365–1383. https://doi.org/10.1002/rcm.7570

Yoshioka, S., Kitano, Y., 1985. Transformation of aragonite to calcite through heating. Geochemical Journal 19, 245–249. https://doi.org/10.2343/geochemj.19.245

Zinke, J., Cantin, N.E., DeLong, K.L., Palmer, K., Boom, A., Hajdas, I., Duprey, N., Martínez-García, A., Rose, N.L., Roberts, S.L., Yang, H., Roberts, L.R., Cundy, A.B., Gaca, P., Milton, J.A., Frank, G., Cox, A., Sampson, S., Tyrrell, G., Agg, M., Turner, S.D., 2023. North Flinders Reef (Coral Sea, Australia) Porites sp. corals as a candidate Global boundary Stratotype Section and Point for the Anthropocene series. The Anthropocene Review 10, 201–224. https://doi.org/10.1177/20530196221142963

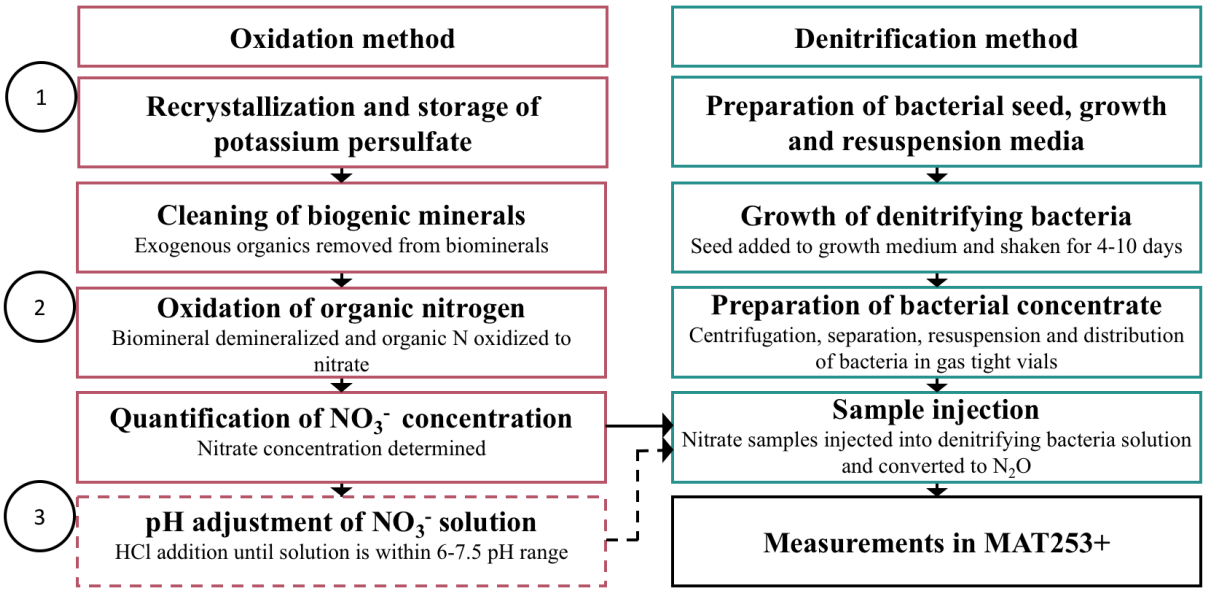

Fig. 1. Summary of steps of oxidation-denitrifier (O-D) method. The steps are summarized in a sequential manner for both the oxidation (red) and denitrifier methods (green). Side arrows connect steps that are co-occurring between the oxidation and the denitrification parts of the method. Preparation of bacterial seed, growth and resuspension media, as well as preparation of bacterial concentrate and injections (green) are discussed extensively in Weigand et al., (2016). Numbered circles refer to the methodological improvements discussed in this work. Dashed outline on the pH adjustment box refer to methodological improvements discussed in this work that allow to bypass pH adjustment of the NO_3^- solutions amended to denitrifying bacteria (Section 2.1).

Fig. 2. Experimental setup for sealing reaction vials during the oxidative conversion of organic nitrogen to nitrate. To seal vials during conversion, up to 120 vials are placed in an aluminum rack and covered with a 0.1 mm thick Teflon sheet followed by a silicon mat. This stack is squeezed between two aluminum plates by means of threaded bolts to provide a good seal on all vials simultaneously. This setup substitutes the previously used phenolic caps that were manually lined with 0.1 mm PTFE septa. By making use of easily accessible materials, it represents a cost-effective setup that reduces consumables costs and increase sample throughput.

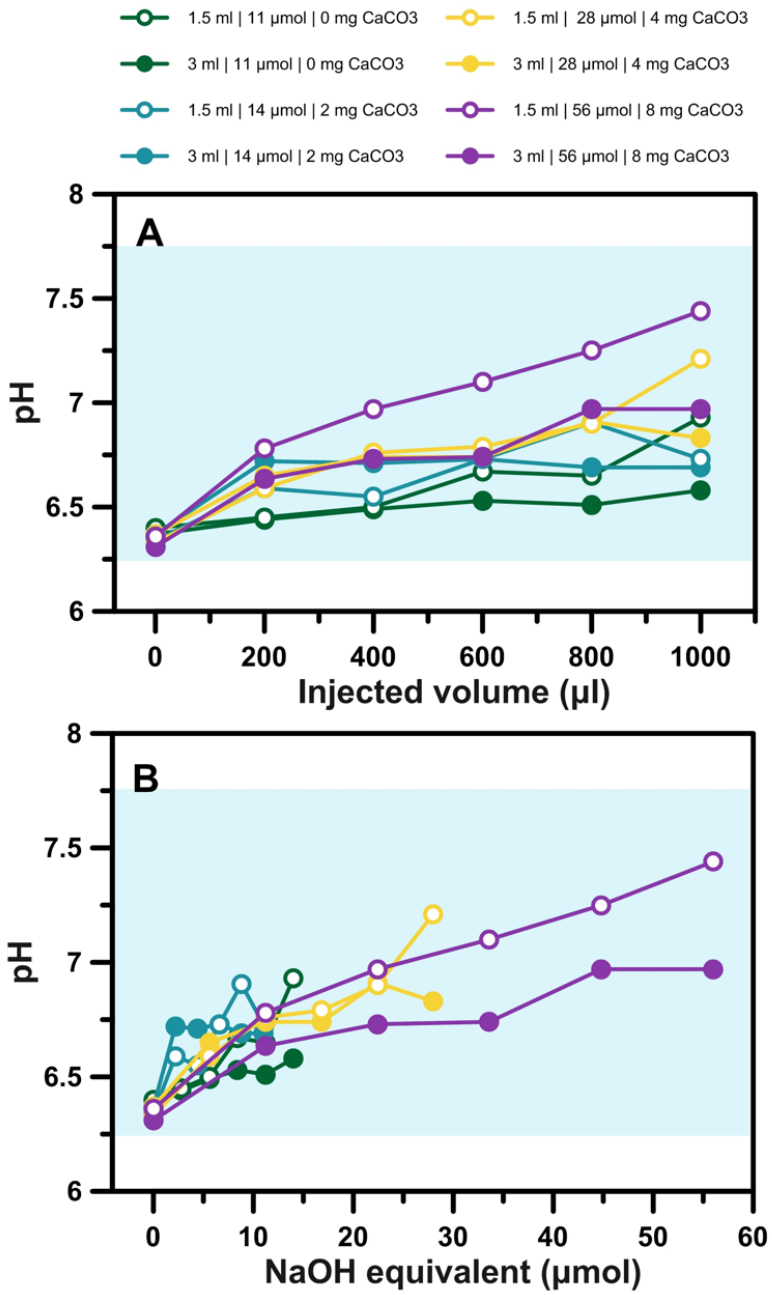

Fig. 3. Testing the pH buffering capacity of freshly harvested *P. chlororaphis* using potassium phosphate monobasic (**A**) pH change of the solution inside the headspace vial after sample amendment of different amounts of POR-oxidized solution. The impact of four different carbonate sample sizes (0, 2, 4 and 8 mg) corresponding to four equivalent excess NaOH injection amounts (11, 14, 28 and 56 µmol respectively) using two different volumes of volume of bacteria resuspension media, 1.5 ml (open symbols) and 3 ml (closed symbols). (**B**) Same dataset plotted against the corresponding injected excess NaOH content. Blue shading represents typical physiological pH range for *P. chlororaphis*.

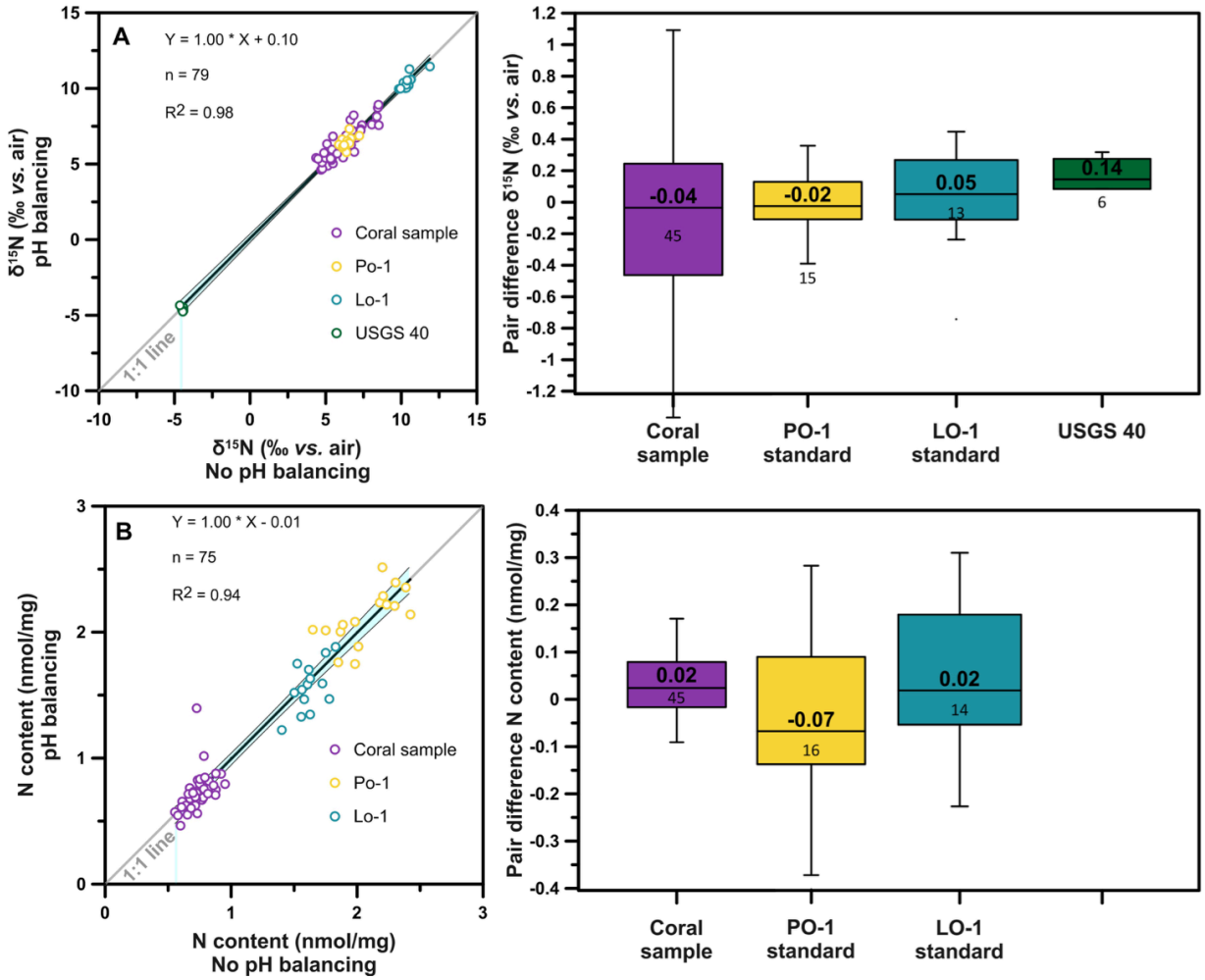

Fig. 4. Evaluation of the effect of bypassing the pH balancing step on $\delta^{15}N$ and weight-normalized N content. (**A**) Left – Cross-plot of $\delta^{15}N$ (‰ *vs.* air) results of biomineral-bound and amino acid RM material. Grey line represents the theoretical 1:1 line (no difference), while the black line represent a least squares linear regression. Blue shading represents the 95 % confidence interval of the regression. Right – box plots depicting the median difference between pH-adjusted and non pH-adjusted sample/RM pairs, with interquartile range (IQR) and vertical bars represented as 1.5 * IQR. (**B**) Same as panel (A) but for weight-normalized biomineral N content (nmol / mg). As amino acid RM USGS 40 is not biomineral-bound, N content data is not provided.

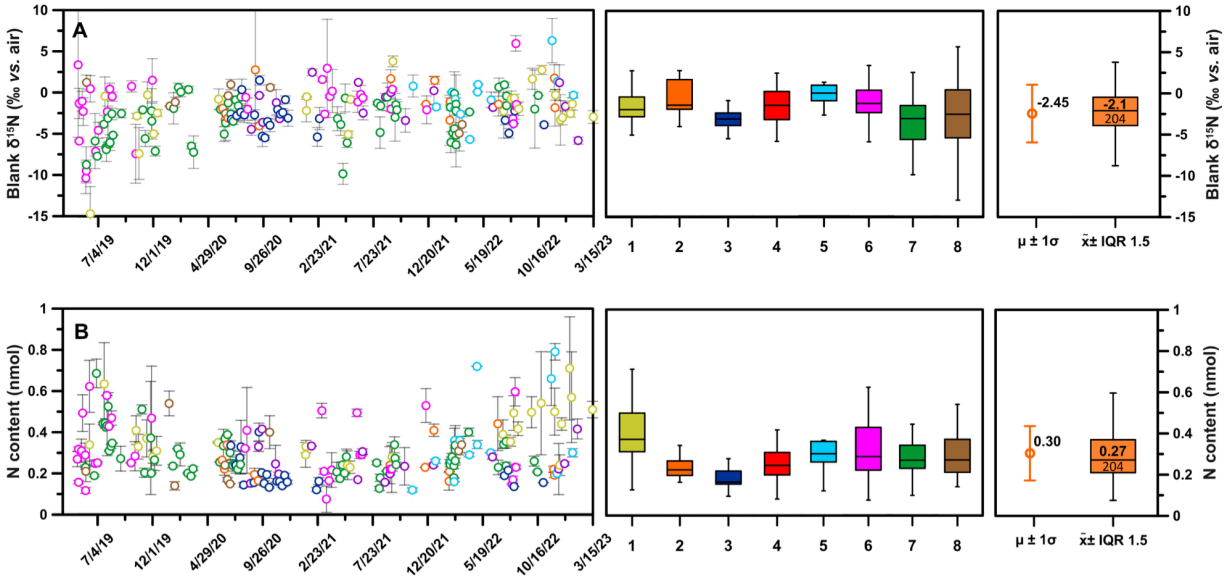

Fig. 5. Evaluation of $\delta^{15}N$ and N content of oxidation blanks at MPIC over the 2019–2023 period. (**A**) Left – Blank $\delta^{15}N$ (‰ *vs.* air) results over the time 2019–2023 for eight individual users using the same color code as ins the central panel. Vertical bars represent 1σ envelope. Center – box plots for individual user datasets with median value, interquartile range (IQR) and vertical bars represented as 1.5 * IQR. Right – Whole-laboratory $\delta^{15}N$ and N content mean (μ) and 1σ as well as conventional box plots with median ($\tilde{x}$), IQR and vertical bars represented as 1.5 * IQR. (**B**) Same as panel (A) but for oxidation blank N content (nmol). While a small user-dependent variability is observed, for most users there are no statistically significant differences.

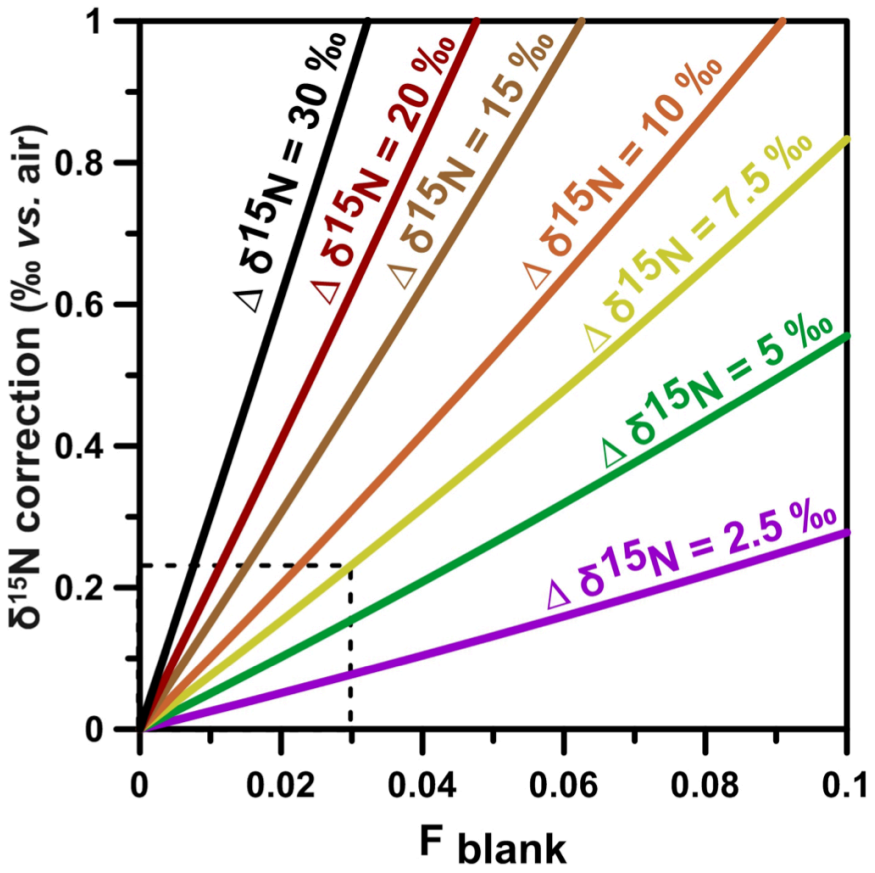

Fig. 6. Theoretical calculation of the oxidation blank correction. Different lines depict the magnitude of $\delta^{15}N$ correction (corrected $\delta^{15}N$ – measured $\delta^{15}N$) applied to BB-$\delta^{15}N$ measurements with the O-D method as a function of F_{blank} [N content $_{blank}$ / (N content $_{sample}$ – N content $_{blank}$)] for varying offsets between the $\delta^{15}N$ of the blank and that of any given sample to be corrected ($\Delta\delta^{15}N$). The dashed line indicates the typical magnitude of $\delta^{15}N$ correction (~ 0.2 ‰) for an average F_{blank} (0.03) and $\Delta\delta^{15}N$ (~ 7.5 ‰) as observed in our long-term study.

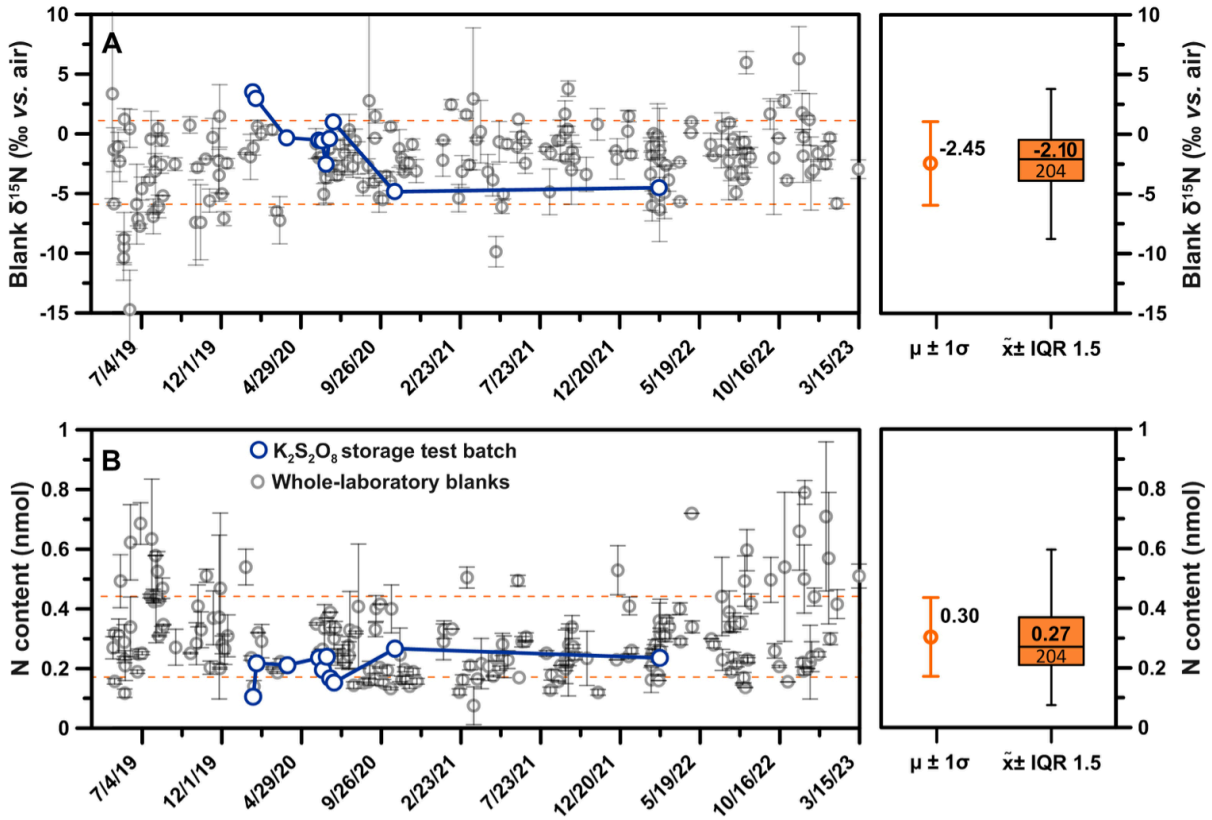

910 **Fig. 7. Long-term storage of dipotassium peroxodisulphate crystals in Ar atmosphere and its effect on oxidation blanks.** (**A**) Left – timeseries of oxidation blanks $\delta^{15}N$ for all users (grey circles) and for a single batch of re-crystalized $K_2S_2O_8$ (blue circles). Orange dashed lines indicate ± 1σ around the mean whole-lab mean. Right – mean (μ) and 1 standard deviation (σ), as depicted in the right panel, which also includes conventional box plots with median ($\tilde{x}$), the interquartile
915 range (IQR) and the error represented as 1.5 the IQR. Dashed lines represent 1σ envelope around the mean whole-laboratory mean. (**B**) Same as panel (A) but for N content (nmol) of the oxidation blanks.

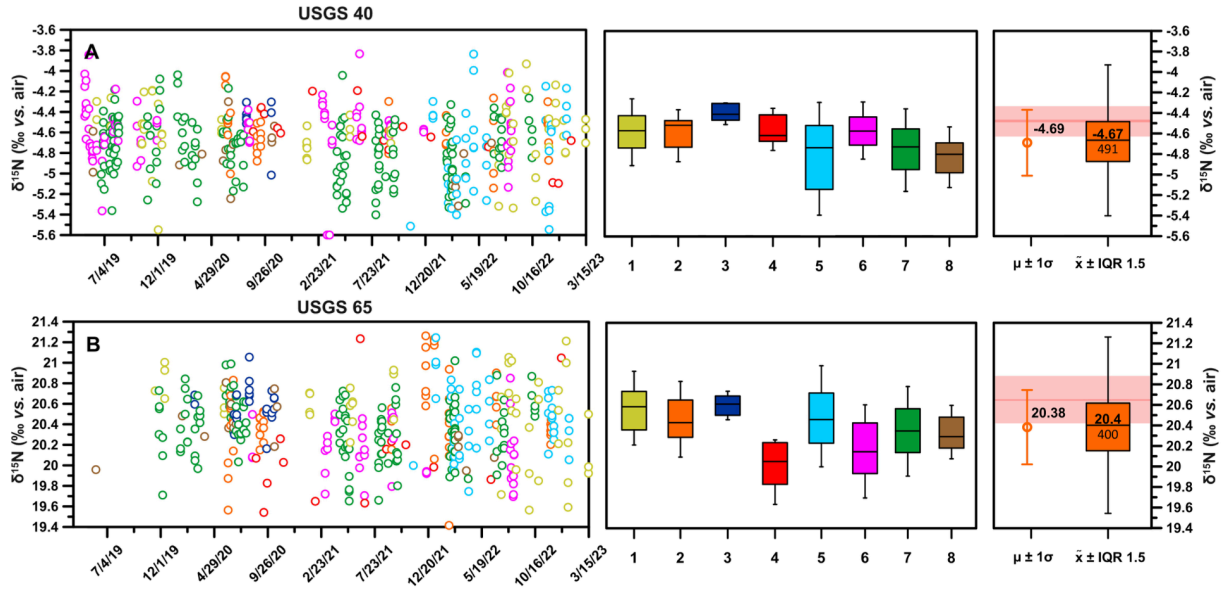

Fig. 8. Evaluation of the long-term precision and accuracy of the O-D method at MPIC over the 2019–2023 period using two international reference amino acid reference materials. (A) Left – $\delta^{15}N$ (‰ *vs.* air) results for USGS 40 RM over ~ 3.5 years for eight individual lab users at MPIC. Middle – box plots for individual users with median, IQR and vertical bars represented as 1.5 * IQR. Right – whole-laboratory (all users) $\delta^{15}N$ values reported as mean (μ) and 1 standard deviation (σ) as well as conventional box plots with median ($\tilde{x}$), IQR and vertical bars represented as 1.5 * IQR. (**B**) Same as panel (A) for USGS 65. Red line and shading in the rightmost panels (A) and (B) represent the international reference values with recalculated uncertainties in 1σ.

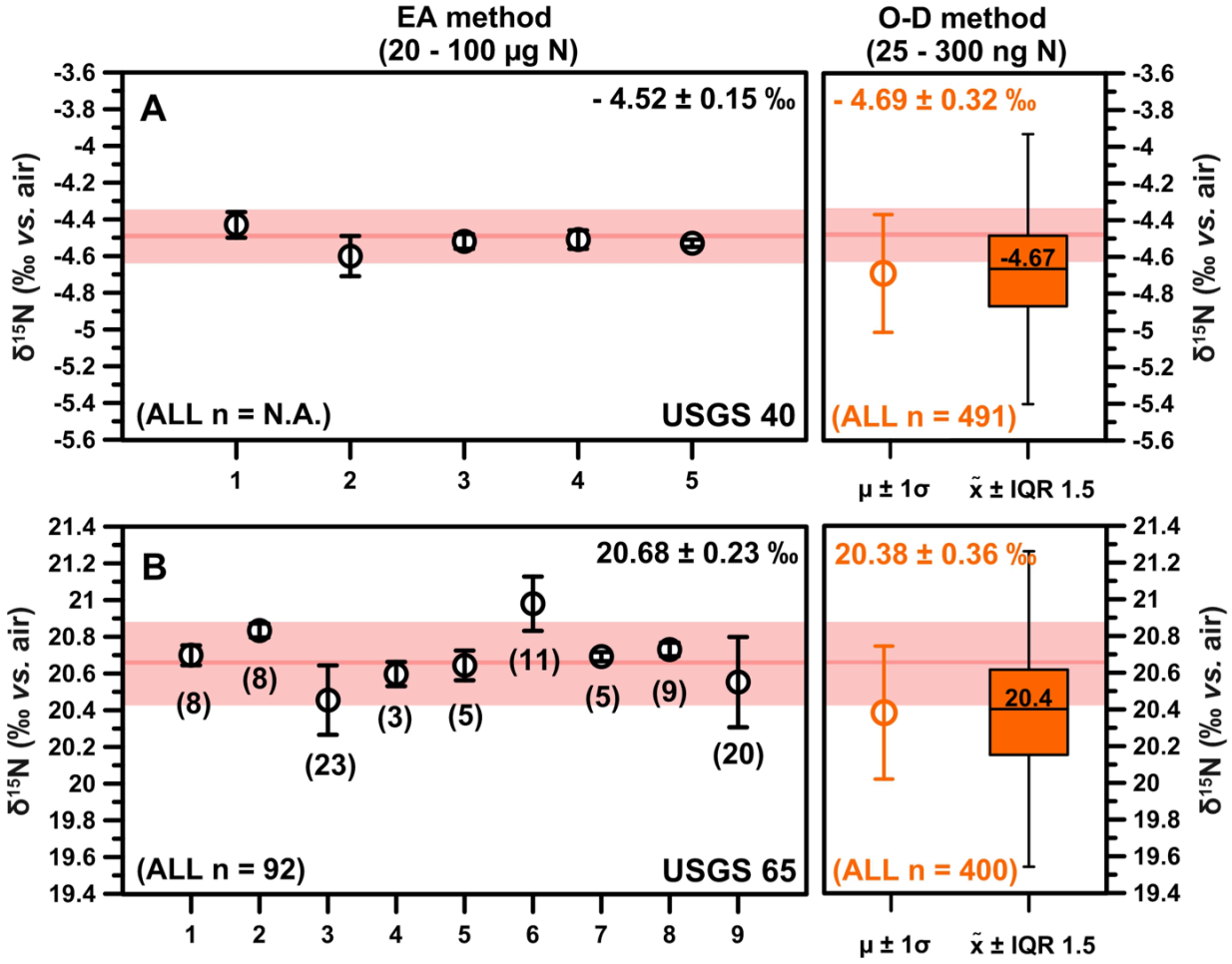

Fig. 9. Published inter-laboratory analyses of $\delta^{15}N$ in amino acid reference materials USGS 40 and 65. (**A**) Left – 1 to 3 represent 3 measurement sessions in one laboratory and 4 to 5 for different laboratory for USGS 40. Vertical bars represent 1σ uncertainty. Right – box plot for MPIC whole-laboratory $\delta^{15}N$ values reported in mean (μ) and 1 standard deviation (σ) as well as conventional box plots with median ($\tilde{x}$), IQR and vertical bars represented as 1.5 * IQR in orange. Red line represents reported reference value in Qi et al., 2013. As individual measurements were not available, recalculated uncertainty with error propagation $\sigma_\mu = \sqrt{{\sigma_1}^2 + {\sigma_2}^2 + \cdots + {\sigma_5}^2}$ of the individual means is applied. (**B**) Left – Nine independent laboratories contributed to $\delta^{15}N$ analysis of USGS 65 with EA techniques for a total of 92 measurements (Schimmelmann et al., 2016). Vertical bars represent 1σ uncertainty and values between brackets are the reported number of measurements for each lab. The total uncertainty (1σ) is recalculated on the mean of the whole dataset (n=92). Right – same as in (A) but for USGS 65.

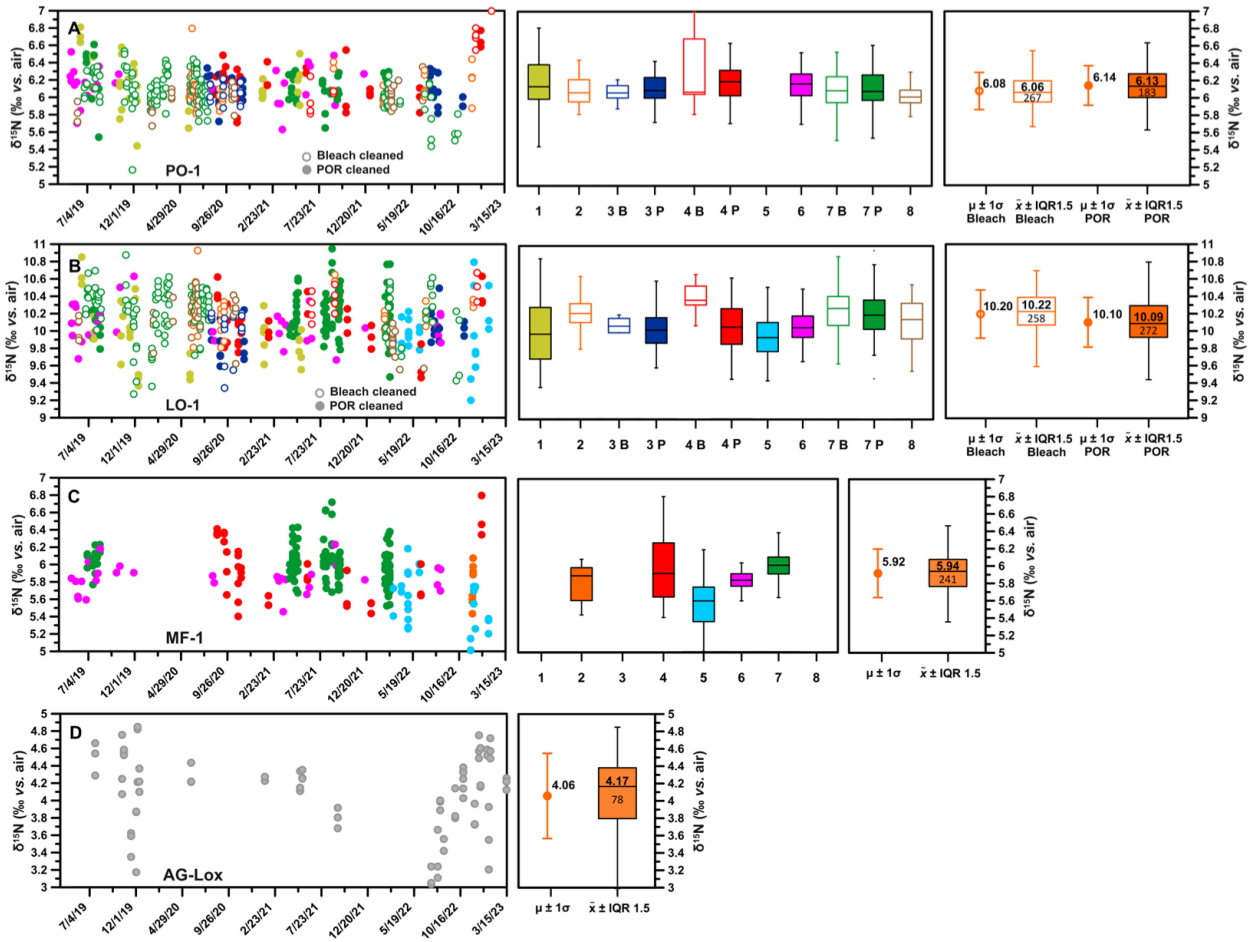

Fig. 10. Evaluation of the long-term analytical precision of BB-δ^{15}N measurements of four biomineral in-house reference materials using the O-D method at MPIC over the 2019–2023 period. (A) Left – BB-δ^{15}N (‰ *vs.* air) results from NaOCl (open symbols) and POR-cleaned (filled symbols) PO-1 coral RM over ~ 3.5 years for 8 individual lab users at MPIC. Middle – box plots for individual user datasets with median, IQR and vertical bars represented as 1.5 * IQR for POR-cleaning (filled box, P) and for NaOCl-cleaning (empty box, B). Right – whole-laboratory (all users) δ^{15}N values reported in mean (μ) and 1 standard deviation (σ) as well as conventional box plots with median ($\tilde{x}$), IQR and vertical bars represented as 1.5 * IQR (**B**) As panel (A) but for NaOCl and POR-cleaned LO-1 coral RM. (**C**) As panel (A) but for POR-cleaned MF-1 foraminifera RM. (**D**) As panel (A) but for POR-cleaned AG-Lox tooth hydroxyapatite RM. The middle panel is not shown here as all measurements were performed by a single user (#1).

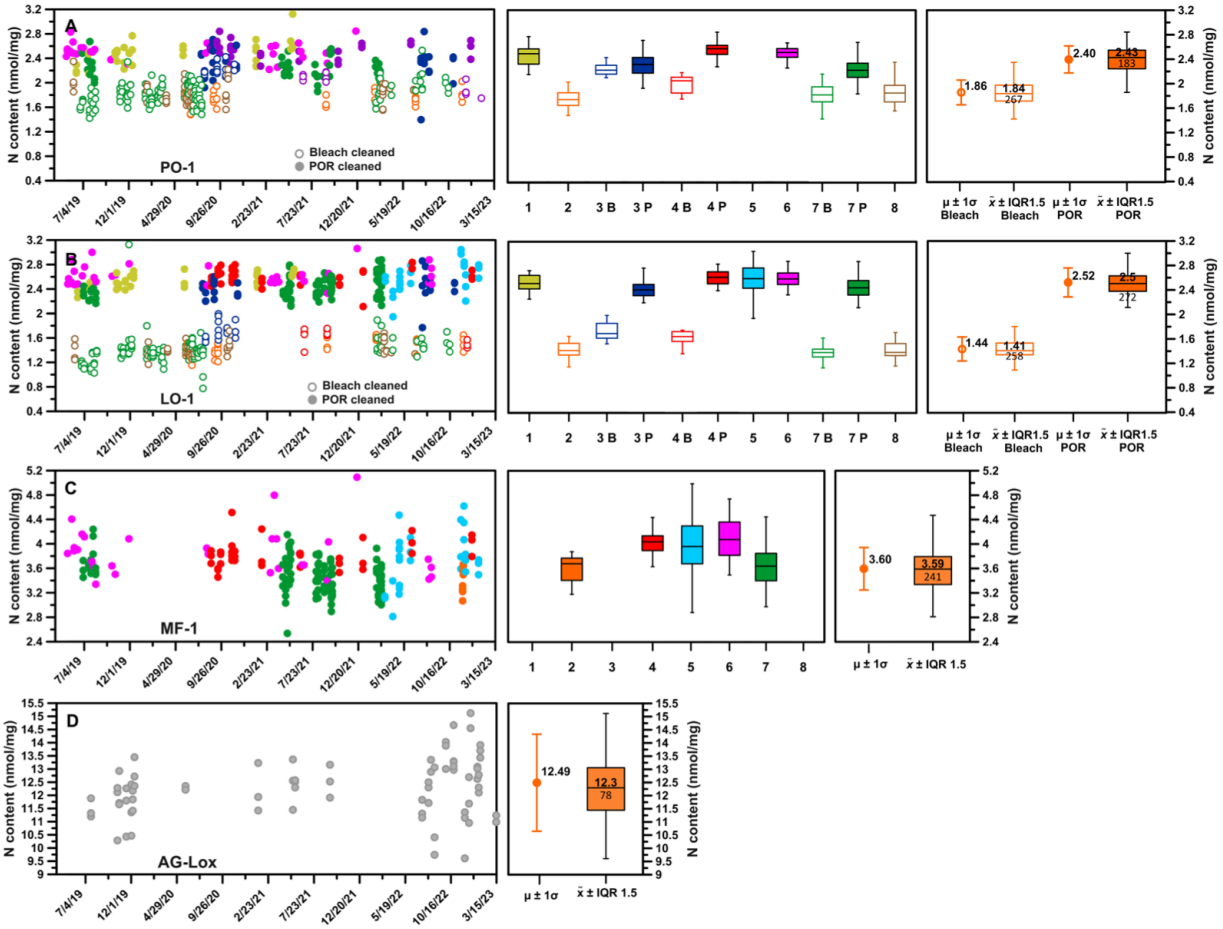

Fig. 11. Evaluation of the long-term analytical precision of weight-normalized N content measurements of four biomineral in-house reference materials using the O-D method at MPIC over the 2019–2023 period. (A) Left – weight-normalized N content (nmol/mg) results from NaOCl (open symbols) and POR-cleaned (filled symbols) PO-1 coral RM over ~ 3.5 years for eight individual lab users at MPIC. Middle – box plots for individual user datasets with median, IQR and vertical bars represented as 1.5 * IQR for POR-cleaning (filled box, P) and for NaOCl-cleaning (empty box, B). Right – whole-laboratory (all users) weight-normalized N content values reported in mean (μ) and 1 standard deviation (σ) as well as conventional box plots with median ($\tilde{x}$), IQR and vertical bars represented as 1.5 * IQR. (**B**) As panel (A) but for NaOCl and POR-cleaned LO-1 coral RM. (**C**) As panel (A) but for POR-cleaned MF-1 foraminifera RM. (**D**) As panel (A) but for POR-cleaned AG-Lox tooth hydroxyapatite RM. The middle panel is not shown here as all measurements were performed by a single user (#1).

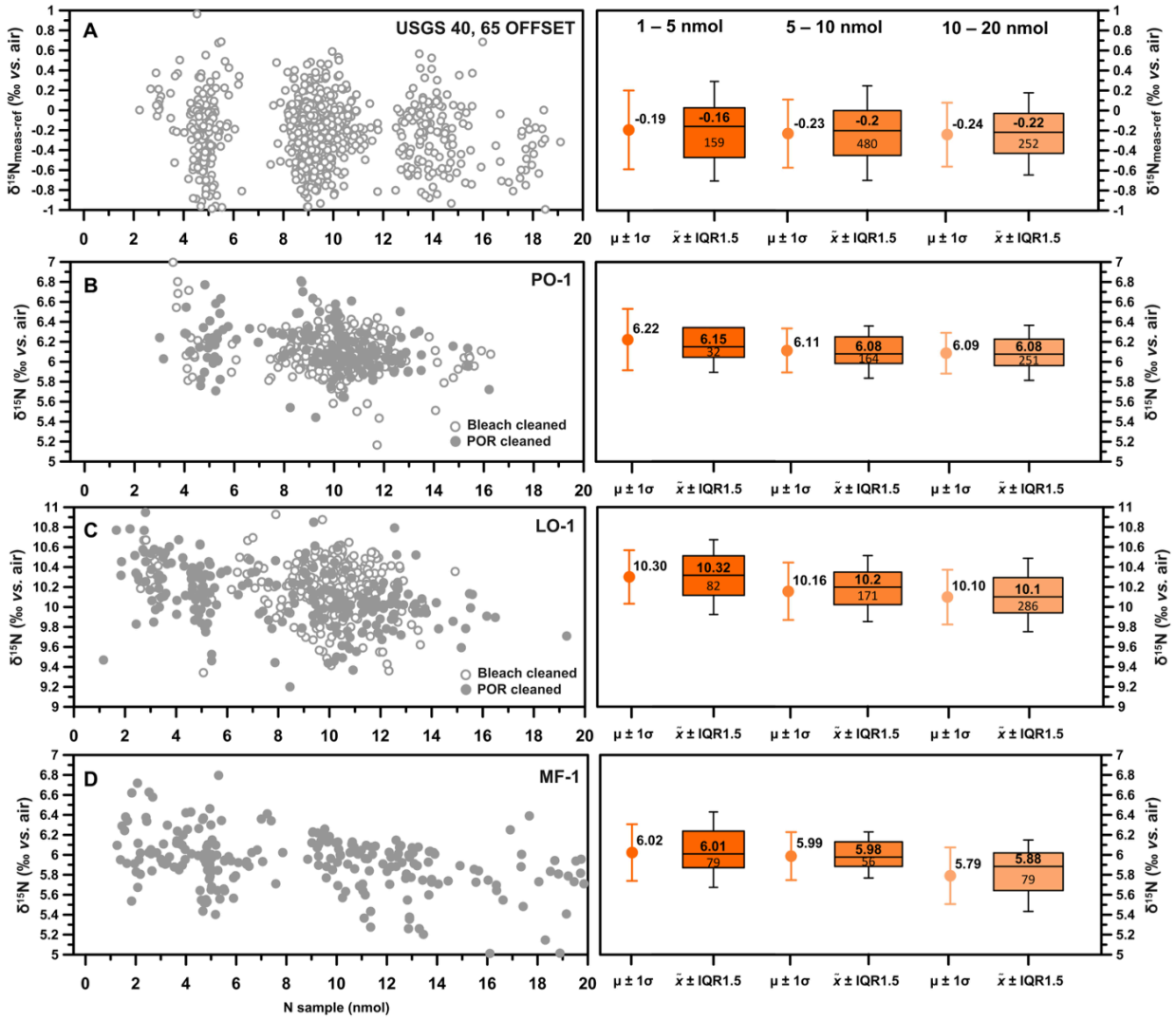

Fig. 12. Evaluation of analytical precession of $\delta^{15}N$ measurements at different concentrations (1–20 nmol) using international reference amino acid and biomineral in-house reference materials. (**A**) Left – combined USGS 40 and 65 offsets from their relative international reference values as a function of sample size (nmol). Right – box plots depicting the median $\delta^{15}N$ (‰ *vs.* air) values for three distinct sample size categories (1–5, 5–10 and 10–20 nmol), reported in mean (μ) and 1 standard deviation (σ) as well as conventional box plots with median ($\tilde{x}$), IQR and vertical bars represented as 1.5 * IQR. (**B, C**) as in (A) but for PO-1 and LO-1 coral RMs. The box plot refers to the combined NaOCl and POR-cleaned datasets. (**D**) As in (A) but for foraminifera MF-1 RM.

Table 1. Recipe for preparation of the "Persulfate oxidizing reagent" from pre-made aliquots.

Step	Reagent	Reference	Amount	Note
Oxidation step	Cleaned biomineral sample	-	0-8 mg	Grain size > 63 µm
Values given for 1 sample	HCl (4M)	Fisher Scientific #11974081	45 µl	Single-use aliquot
	POR	-	1 ml	See composition below
"Persulfate oxidizing Reagent" (POR) [a]	NaOH (6.25 µM)	Acros #383040010 or Fisher Scientific #10106482	4 ml	Single-use aliquot
Values given for 100ml of reagent	$K_2S_2O_8$	Sigma Aldrich #60489	0.7 g	Single-use aliquot packed under Ar atmosphere
	Deionized water	milliQ – millipore	96 ml	-

[a] Persulfate Oxidizing Reagent (POR) is also used as a type of oxidative cleaning that is commonly applied to certain types of biomineral matrices. See section 3.5 for a discussion of cleaning methods.

985

Table 2. List of reference materials used in this study

Reference material ID	Biogenic mineral and source taxa	Cleaning method	Reference
	Amino acids reference materials		
USGS 40	L-Glutamic acid	-	Qi et al., 2003
USGS 65	Glycine	-	Schimmelmann et al., 2016
	In-house biomineral reference materials		
PO-1	$CaCO_3$ (aragonite) *Porites sp.*	POR-cleaned and NaOCl-cleaned	Leichliter et al., 2021
LO-1	$CaCO_3$ (aragonite) *Lophelia pertusa*	POR-cleaned and NaOCl-cleaned	Leichliter et al., 2021
AG-Lox	$Ca_5(PO_4)_3(OH)$ (hydroxyapatite) *Loxodonta africana*	POR-cleaned	Leichliter et al., 2021
MF-1	$CaCO_3$ (calcite) Mixed North Atlantic foraminifera	POR-cleaned	Martínez-García et al., 2022
	Nitrate reference materials		
IAEA-NO3	KNO_3^-	-	Böhlke & Coplen, 1995
USGS34	KNO_3^-	-	Böhlke et al., 2003

Table 3. Comparison of pH adjusted and non pH adjusted materials and their statistical significance

	Coral sample [a]	**PO-1**	**LO-1**	**USGS40**
	$\delta^{15}N$ (‰ *vs.* air)			
$\delta^{15}N$ no – pH adjust (‰)	6.15 ± 1.15	6.37 ± 0.32	10.45 ± 0.50	– 4.48 ± 0.036
$\delta^{15}N$ pH adjust (‰)	6.30 ± 1.12	6.39 ± 0.36	10.42 ± 0.46	– 4.59 ± 0.15
n	45	15	13	6
Mean difference (‰) [b]	0.14 ± 1.60	0.02 ± 0.49	– 0.03 ± 0.67	– 0.11 ± 0.17
P value [c]	0.5482	0.8866	0.8749	0.1364
	Weight-normalized N content (nmol/mg)			
N content no pH	0.73 ± 0.09	2.08 ± 0.24	1.62 ± 0.12	-
N content pH	0.72 ± 0.15	2.12 ± 0.22	1.56 ± 0.19	-
n	45	16	14	-
Mean difference (nmol/mg) [b]	– 0.01 ± 0.17	0.04 ± 0.32	– 0.06 ± 0.22	-
P value [c]	0.6999	0.5846	0.3428	-

[a] *Pocillopora damicornis* (Linnnaeus, 1758), non homogeneized sample matrix.

[b] Propagated error calculated as $\sigma_{1-2} = \sqrt{{\sigma_1}^2 + {\sigma_2}^2}$. Note that Fig. 4 shows a box plot visualization of the median of the individual pairs, while here the difference is reported across whole categories averages. In both cases differences are always < 0.15 for both $\delta^{15}N$ (‰ *vs.* air) and weight-normalized N content (nmol/mg).

[c] Double-tailed unpaired t-test with α<0.05

Table 4. Observed $\delta^{15}N$ and N content values for blanks and reference materials

ID	Material	$\delta^{15}N$ (‰ *vs.* air)	N content (nmol or nmol / mg) [a]
	Oxidation blanks and amino acids reference materials		
Blanks	POR	– 2.45 ± 3.50 (n=204)	0.30 ± 0.13 (n=204)
USGS 40	L-Glutamic acid	– 4.69 ± 0.32 (n=491)	-
USGS 65	Glycine	20.38 ± 0.36 (n=400)	-
OFFSET USGS 40, 65 [b]	L-Glutamic acid and Glycine	– 0.23 ± 0.35 (n=891)	-
	In-house biomineral reference materials		
PO-1	$CaCO_3$ (aragonite) POR-cleaned	6.14 ± 0.23 (n=183)	2.40 ± 0.22 (n=183)
PO-1	$CaCO_3$ (aragonite) NaOCl-cleaned	6.08 ± 0.21 (n=267)	1.86 ± 0.20 (n=267)
LO-1	$CaCO_3$ (aragonite) POR-cleaned	10.10 ± 0.29 (n=272)	2.52 ± 0.24 (n=272)
LO-1	$CaCO_3$ (aragonite) NaOCl-cleaned	10.20 ± 0.28 (n=258)	1.44 ± 0.20 (n=258)
MF-1	$CaCO_3$ (calcite) POR-cleaned	5.92 ± 0.28 (n=243)	3.60 ± 0.35 (n=241)
AG-Lox	$Ca_5(PO_4)_3(OH)$ (hydroxyapatite) POR-cleaned	4.06 ± 0.49 (n=78)	12.49 ± 1.85 (n=78)

[a] For biominerals, N content is reported as weight-normalized N content (nmol of N per milligram of cleaned biomineral material).

[b] Offsets reported from the respective international reference values (Qi et al., 2003; Schimmelmann et al., 2016).

Table 5. NaOCl *vs.* POR-cleaned PO-1 and LO-1 reference materials

	PO-1	LO-1
	$\delta^{15}N$ (‰ *vs.* air)	
$\delta^{15}N$ NaOCl cleaning	6.08 ± 0.21 (n=267)	10.20 ± 0.28 (n=258)
$\delta^{15}N$ POR cleaning	6.14 ± 0.23 (n=183)	10.10 ± 0.29 (n=272)
Mean difference (‰) [a]	0.06 ± 0.31	-0.09 ± 0.40
P value [b]	***0.0028***	***0.0001***
	Weight-normalized N content (nmol/mg)	
N content NaOCl cleaning	1.86 ± 0.20 (n=267)	1.44 ± 0.20 (n=258)
N content POR cleaning	2.40 ± 0.22 (n=183)	2.52 ± 0.24 (n=272)
Mean difference (nmol/mg) [a]	0.54 ± 0.30 (n=183)	1.08 ± 0.31 (n=272)
P value [b]	***<0.0001***	***<0.0001***

[a] Propagated error calculated as $\sigma_{1-2} = \sqrt{{\sigma_1}^2 + {\sigma_2}^2}$, values in ‰ *vs.* air.

[b] Double-tailed unpaired t-test with α<0.05, bold italics values represent statistically significant differences.

Table 6. Comparison of $\delta^{15}N$ differences across sample size categories of measured reference materials

	n1, n2, n3 [a]	**1–5 nmol**	**5–10 nmol**	**10–20 nmol**
		Mean value		
PO-1	32, 164, 251	6.22 ± 0.31 ‰	6.11 ± 0.22 ‰	6.09 ± 0.21 ‰
LO-1	79, 168, 283	10.30 ± 0.27 ‰	10.16 ± 0.29 ‰	10.10 ± 0.27 ‰
MF-1	78, 55, 78	6.02 ± 0.28 ‰	5.99 ± 0.24 ‰	5.79 ± 0.28 ‰
USGS 40 + 65 offsets	159, 480, 252	– 0.19 ± 0.40 ‰	– 0.23 ± 0.34 ‰	– 0.24 ± 0.32 ‰
	n1, n2, n3 [a]	**1–5 *vs.* 5–10 nmol**	**1–5 *vs.* 10–20 nmol**	**5-10 *vs.* 10–20 nmol**
		Mean difference size classes [b]		
PO-1	32, 164, 251	0.11 ± 0.38 ‰	0.14 ± 0.37 ‰	0.03 ± 0.30 ‰
LO-1	79, 168, 283	0.14 ± 0.39 ‰	0.20 ± 0.38 ‰	0.06 ± 0.40 ‰
MF-1	78, 55, 78	0.04 ± 0.37 ‰	0.23 ± 0.40 ‰	0.20 ± 0.37 ‰
USGS 40 + 65 offsets	159, 480, 252	0.04 ± 0.52 ‰	0.05 ± 0.51 ‰	0.01 ± 0.47 ‰

[a] n1 for 1–5 nmol, n2 for 5–10 nmol and n3 for 10–20 nmol.

[b] Propagated error calculated as $\sigma_{1-2} = \sqrt{{\sigma_1}^2 + {\sigma_2}^2}$, values in ‰ *vs.* air.

SUPPLEMENTARY FIGURES:

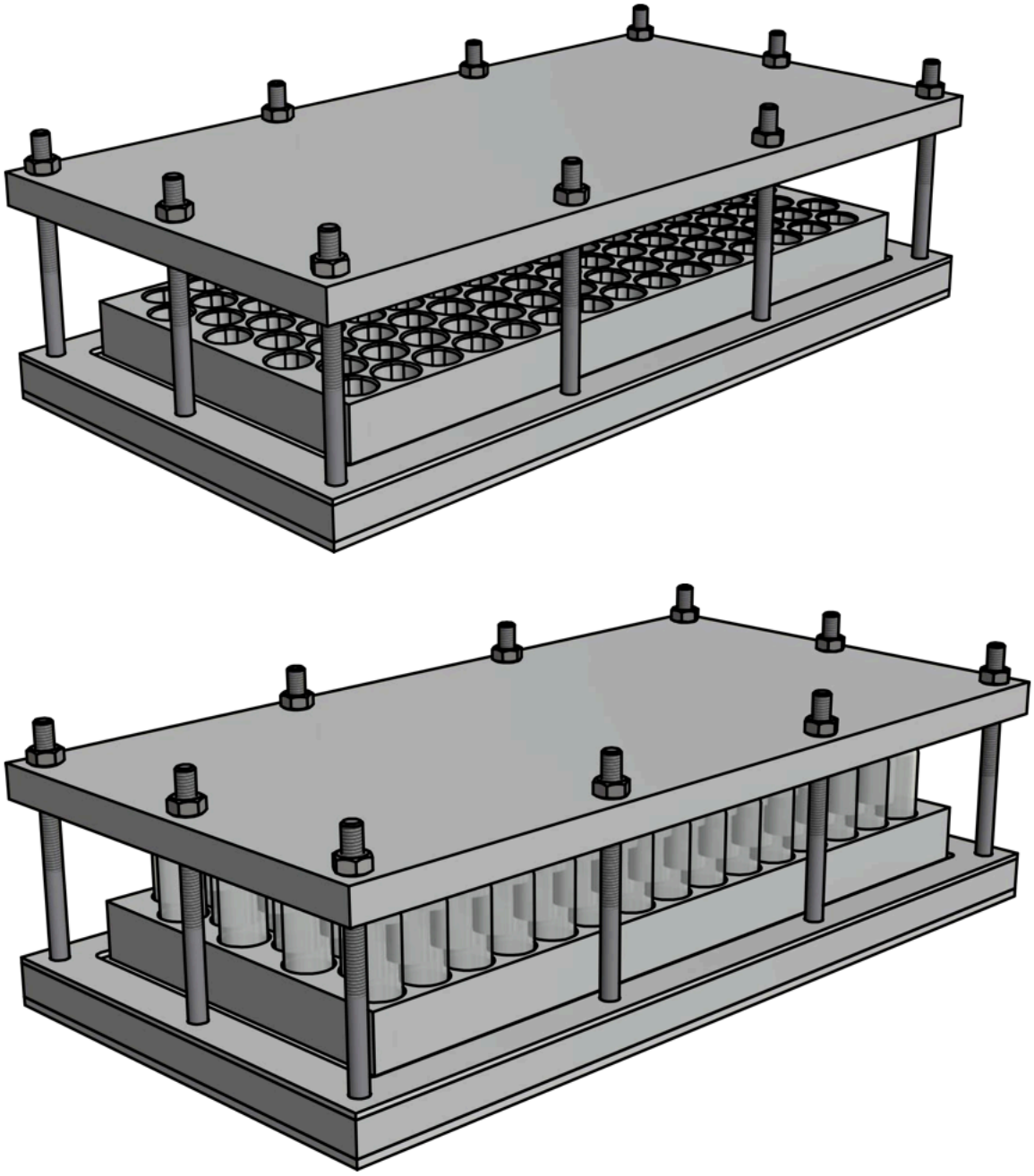

Fig. S1 – Schematics of the "Sandwich" system. The drawing shows the with and without oxidation vials loaded onto the rack. Vials are squeezed between metal plates with the upper plate being lined with a sheet of silicone and 0.1 mm of PTFE material (see Fig. 2, main text). A full 3D Model of the assembly in STEP format is provided in the Supplementary Data.

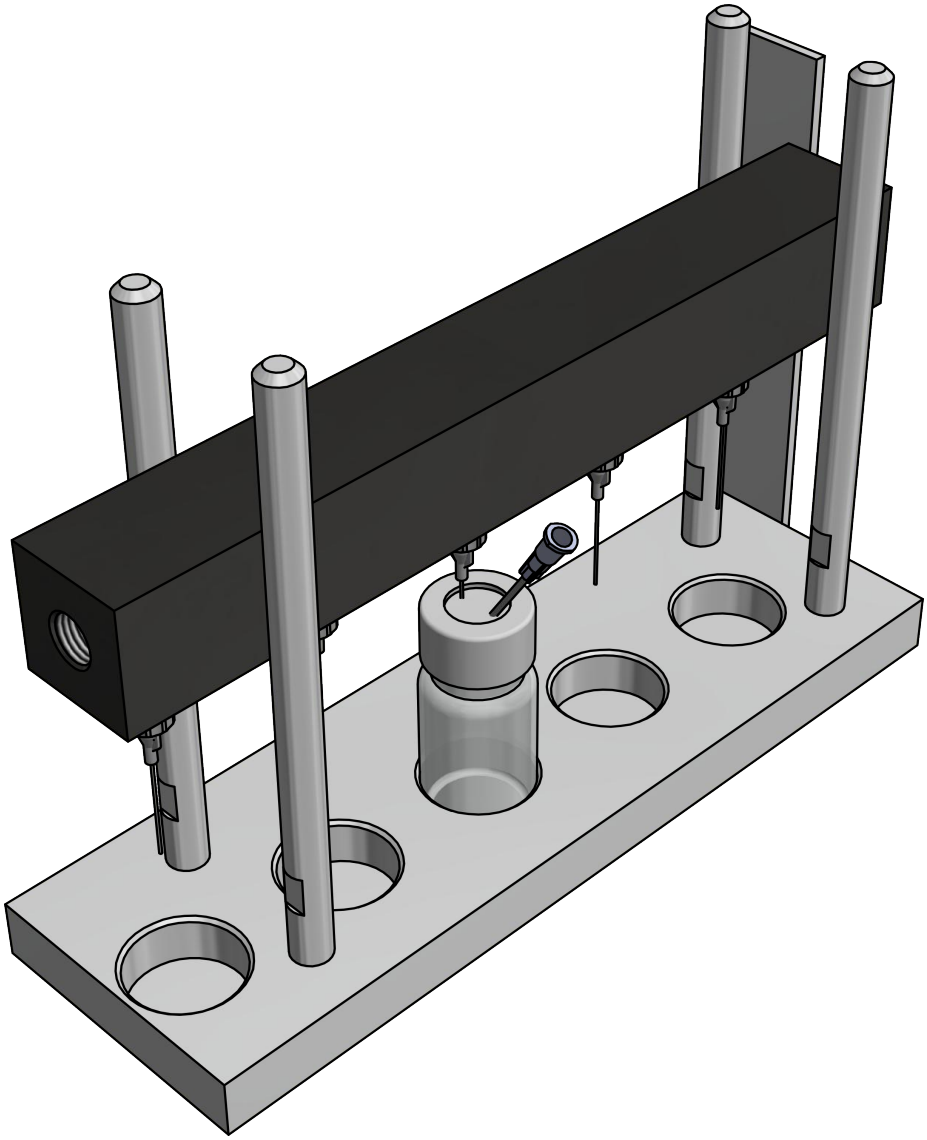

Fig. S2 – Schematics of the Argon purging system for $K_2S_2O_8$ crystal storage. After sealing with a silicone cap with PTFE coating, glass EPA vials containing freshly recrystallized $K_2S_2O_8$ are flushed with Ar in batches of 5 vials for 5 minutes to remove air impurities. For half of this time, a venting needle is also punctured through the septa for purged gasses to escape. A full 3D model in STEP format of the apparatus used to replace the atmosphere in the vials with Ar is provided in the Supplementary Data.

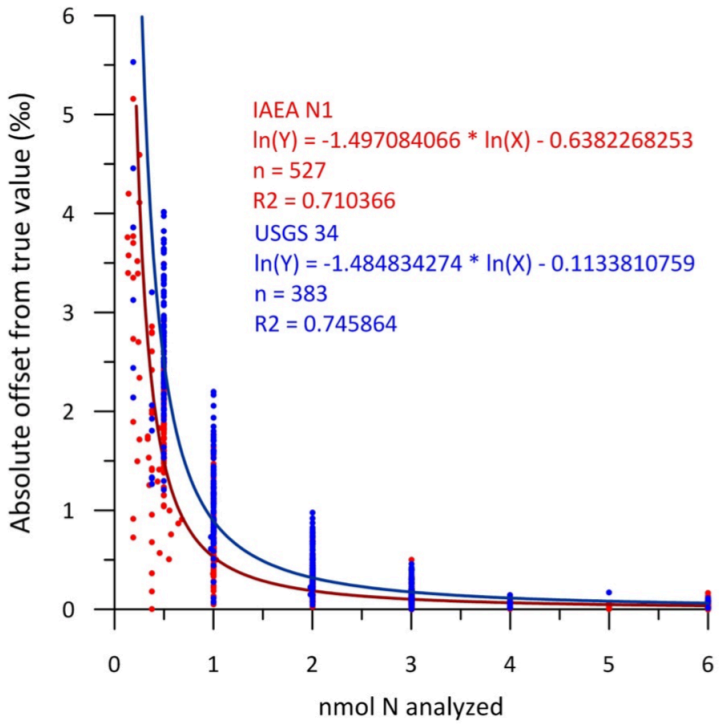

Fig. S3 – Offsets from the true value for different amounts of nitrogen injected to the bacteria for two nitrate reference materials for a single user. Analyses were performed over the course of 2 years by one individual user. Lower amounts of analyte results in a progressively larger offset from the true value as well as a larger scattering of the data. This scatter largely disappears when >3 nmol N are present for analysis.

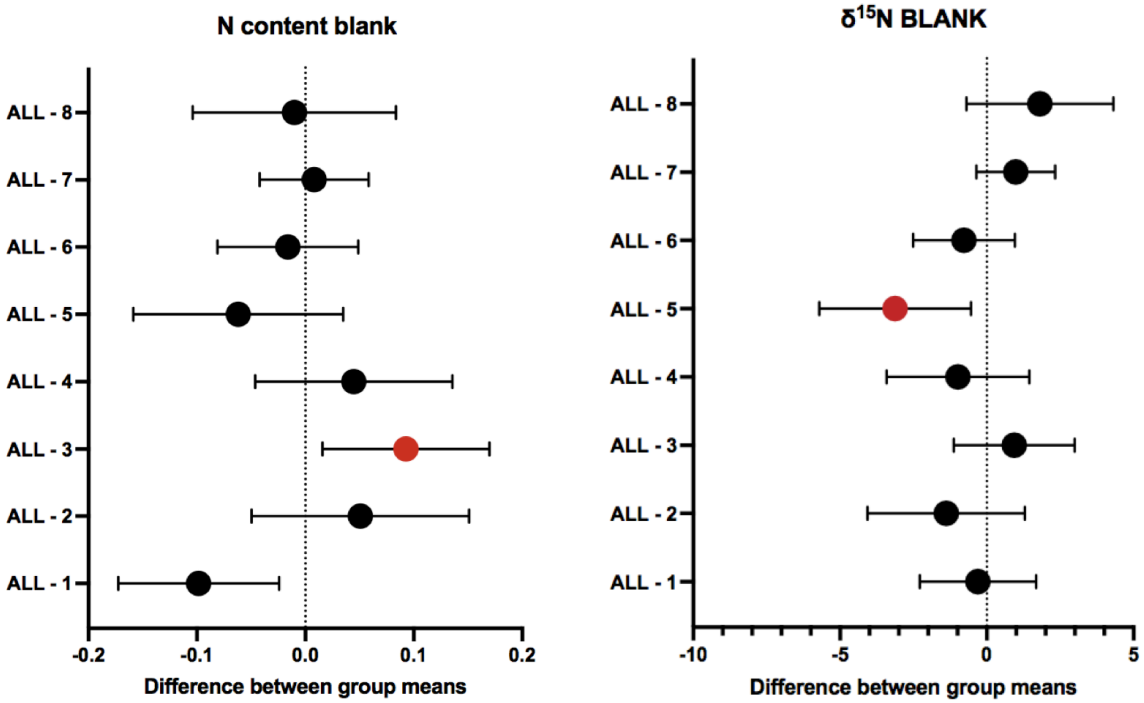

Fig. S4 – One-way Anova test confidence intervals for blanks N content and $\delta^{15}N$. Individual users mean values are compared to the whole-laboratory mean values. Horizontal bars represent 95 % confidence intervals on the mean of individual users. The difference between means is statistically significant if the confidence interval does not intersect the zero mean difference vertical line.

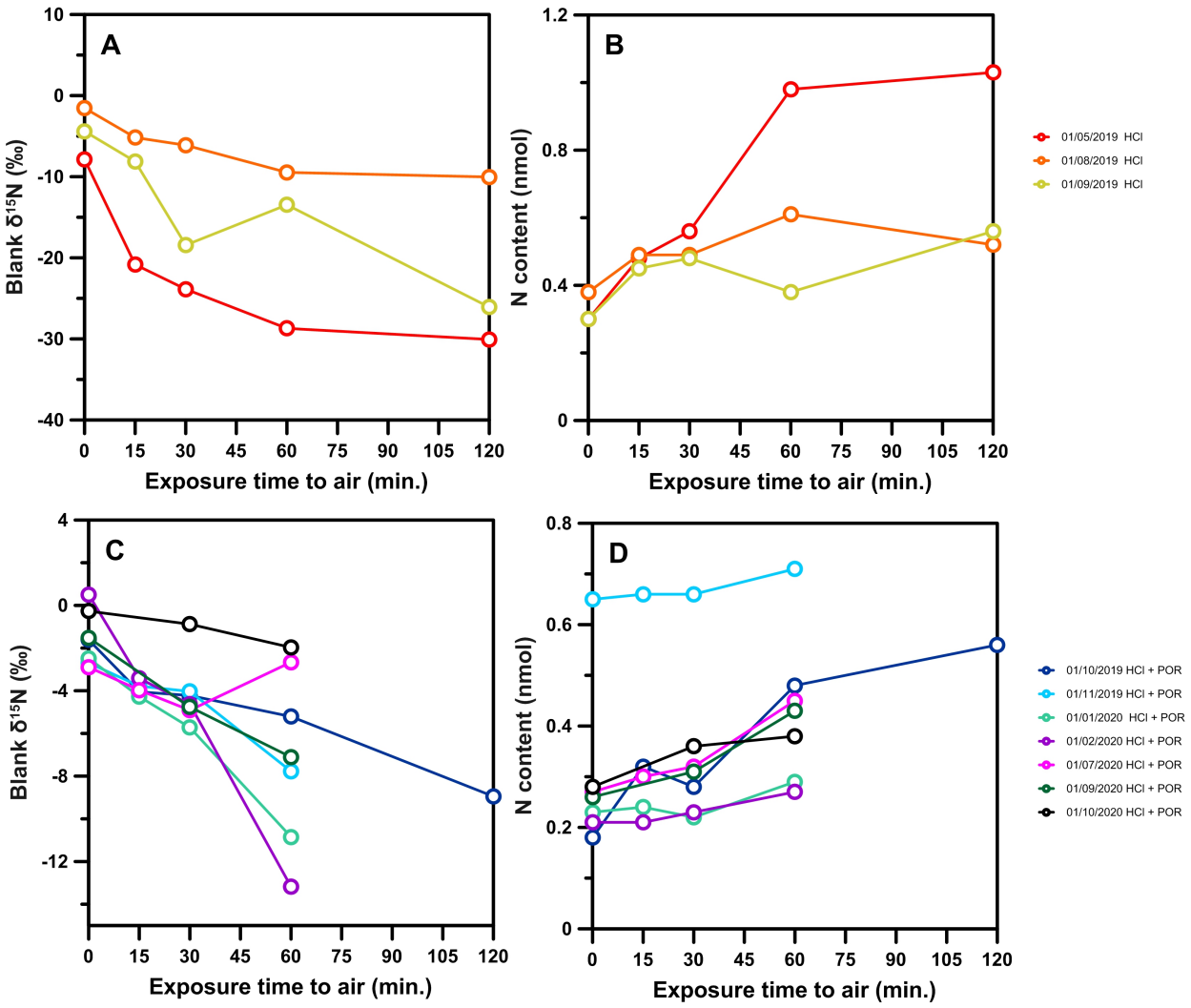

Fig. S5 – Results from air exposure tests for pure HCl and HCl amended with POR and their impact on oxidation blanks (**A**) Time of exposure in minutes of 45 µl of pure 4M HCl versus blanks $\delta^{15}N$ (‰ *vs.* air). POR solution was added after the exposure test was concluded in each case. (**B**) Same dataset as (A) displaying blanks N content (nmol). (**C**) Time of exposure of 45 µl of 4M HCl and 1000 µl of POR solution as routinely amended to samples. (**D**) Same dataset as (C) displaying blanks N content. Each vial was opened for the specified time and then capped with a milliQ-cleaned and PTFE coated cap. Each coloured line represents an exposure experiment performed on a separate day.

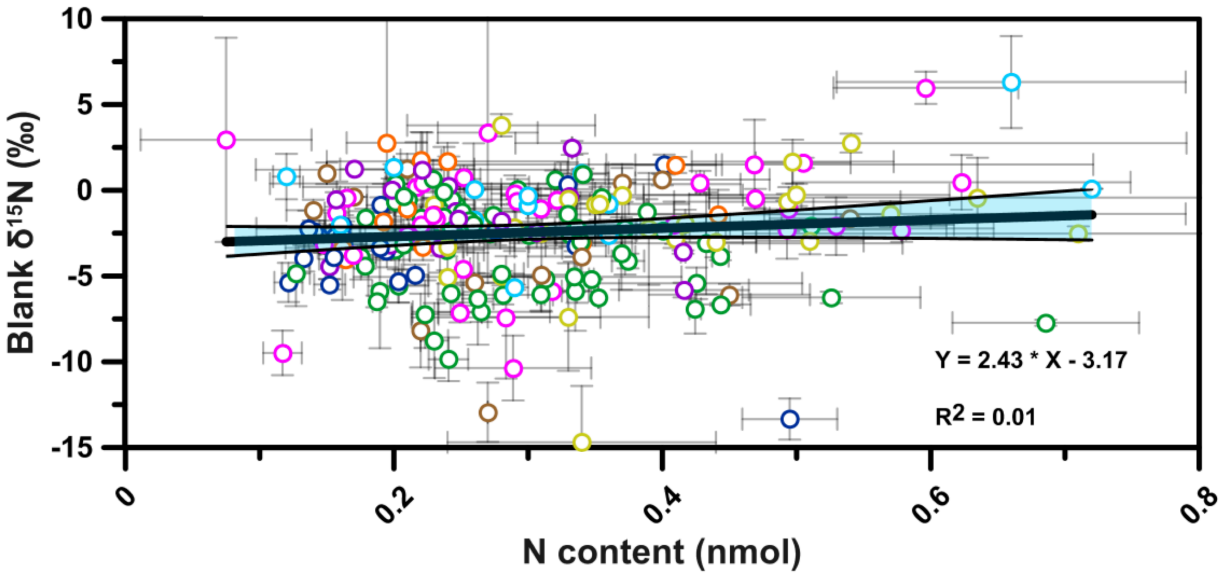

Fig. S6 – Cross-plot of $\delta^{15}N$ and N content for oxidation blanks for all users. No correlation can be observed between oxidation blanks $\delta^{15}N$ and N content across eight different lab users.

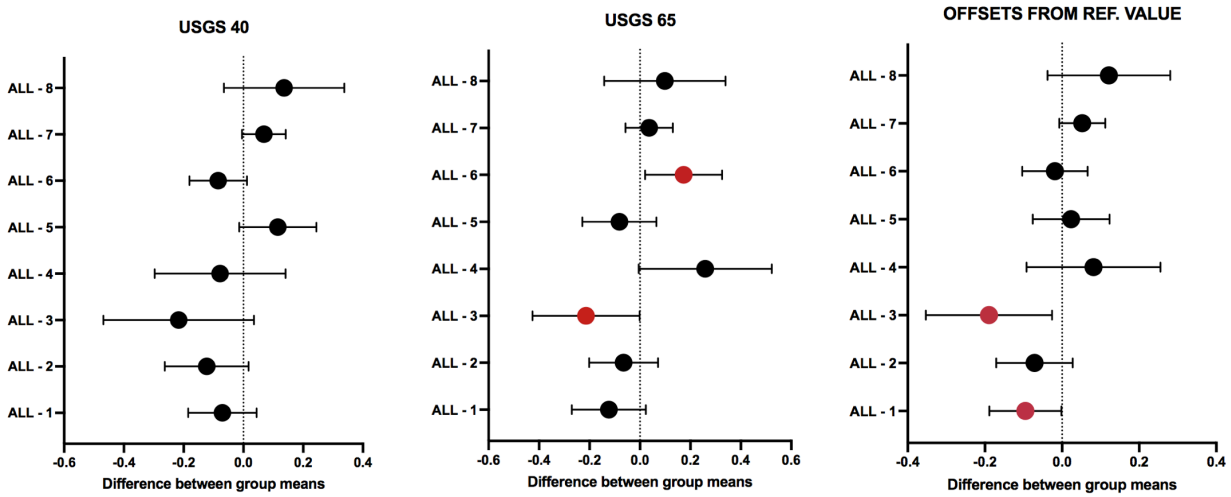

Fig. S7 – One-way Anova test confidence intervals for amino acid reference materials $\delta^{15}N$ difference across users. Individual users mean values are compared to the whole-laboratory mean values. Horizontal bars represent 95 % confidence intervals on the mean of individual users. The difference between means is statistically significant if the confidence interval does not intersect the zero mean difference vertical line.

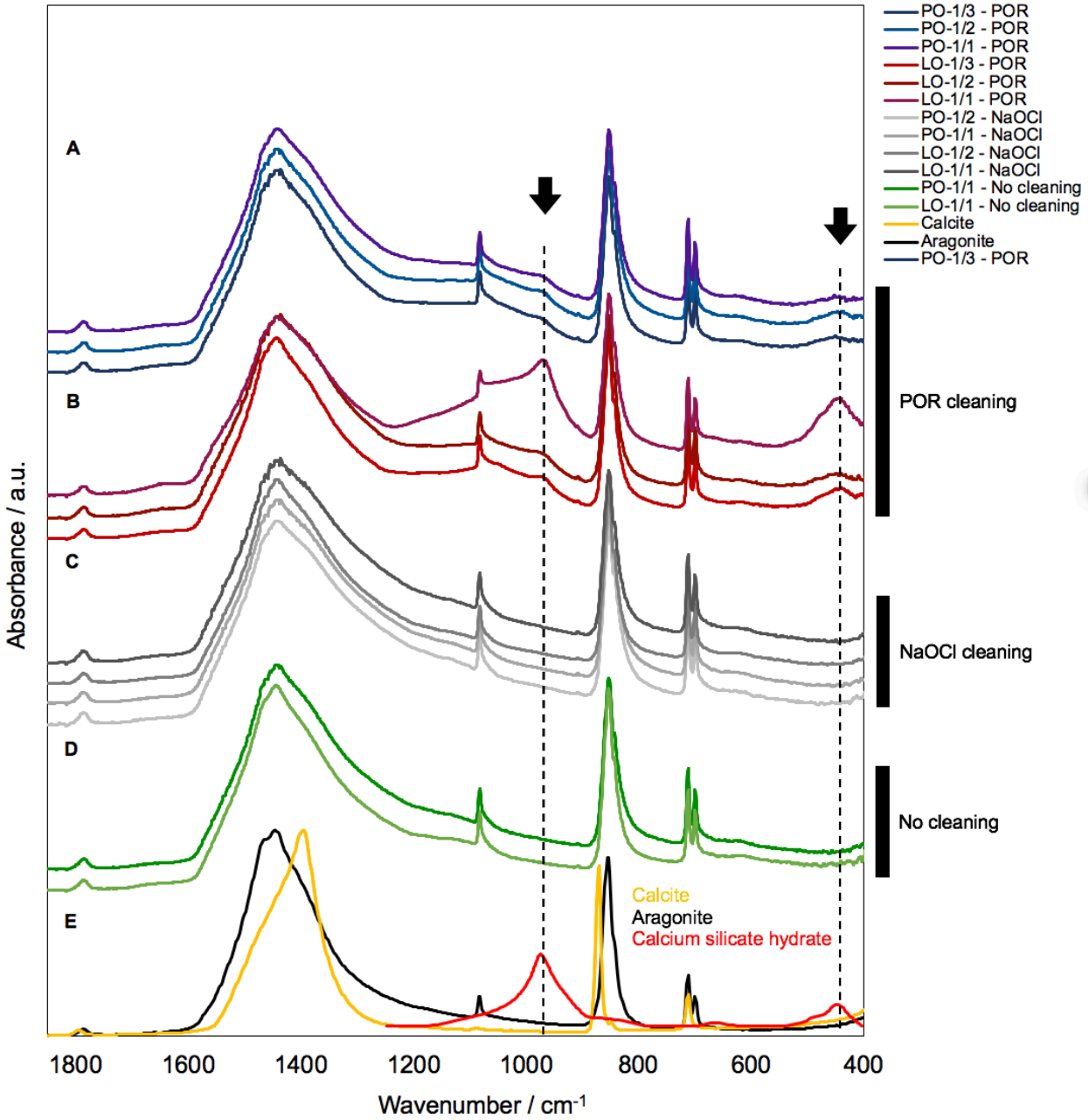

Fig. S8 – FTIR spectra of uncleaned and POR-cleaned PO-1 and LO-1 reference materials. **(A)** Spectra of POR-cleaned LO-1 RM (blue colours). (**B**) Spectra of POR-cleaned PO-1 RMs (red colours). (**C**) Spectra of NaOCl-cleaned LO-1 (dark gray) and PO-1 (light gray) RMs. (**D**) Spectra of uncleaned LO-1 (light green) and PO-1 (dark green) coral RM. (**E**) Reference spectra for Calcite (yellow) and Aragonite (black) and Calcium silicate hydrate (CSH, yellow). CSH spectra from (John and Stephan, 2021). FTIR stands for Fourrier-Transfer Infrared Spectroscopy

Table S1. Cleaning method and recipes used in this study

Step	Reagent	Brand / #Product code	Amount	Note
Reductive and oxidative cleaning	biomineral sample	-	0–15 mg	Grain size > 63 µm
PO-1, LO-1, MF-1, AG-Lox	Na-Polyphosphate 2% in milliQ	Thermo Scientific #390930010	10 ml	-
Values given for 1 sample	Na-Dithionite solution	-	3–7 ml	See composition below
	POR [a]	-	3 ml	See composition below
Oxidative cleaning PO-1 and LO-1 Values given for 1 sample	NaOCl (10-15% active chlorine) [a]	Acros Organics #219255000	4.25 ml	Single bottle opened per batch of samples
Na-Dithionite solution Values given in 100ml of milliQ	Sodium citrate	Fisher Scientific #BP327-1	6.2 g	-
	Sodium bicarbonate	Acros organics #217120010	2 g	-
	Na-Dithionite solution	Fisher Scientific #10274490	5 g	-
	NaOH (4 M)	Acros #383040010 or Fisher Scientific #10106482	400 µl	-
"Persulfate oxidizing Reagent" (POR)	NaOH (6.25 µM)	Acros organics #383040010 or Fisher Scientific #10106482	4 ml	Single-use aliquot
	$K_2S_2O_8$	Sigma Aldrich #60489	0.7 g	Single-use aliquot packed under Ar atmosphere
	Deionized water	milliQ – millipore	96 ml	-

1085

Table S2. One-way Anova test results for comparison of $\delta^{15}N$ differences across sample size categories of measured reference materials

	n1, n2, n3 [a]	**1–5 *vs.* 5–10 nmol**	**1–5 *vs.* 10–20 nmol**	**5–10 *vs.* 10–20 nmol**
		P value [b]		
PO-1	32, 164, 251	***0.0295***	***0.0029***	0.4167
LO-1	79, 168, 283	***0.0005***	***<0.0001***	0.0769
MF-1	78, 55, 78	0.7411	***<0.0001***	***0.0002***
USGS 40 + 65 offsets	159, 480, 252	0.4748	0.3652	0.9178

[a] n1 for 1–5 nmol, n2 for 5–10 nmol and n3 for 10–20 nmol

[b] one-way Anova test with α<0.05, bold italics values represent statistically significant differences.